JOURNAL OF GEOPHYSICAL RESEARCH, VOL. 101, NO. C12, PAGES 28,417–28,439, DECEMBER 15, 1996

Seasonal characteristics of the perennial ice cover of the Beaufort Sea

R. Kwok
Jet Propulsion Laboratory, California Institute of Technology, Pasadena

J. C. Comiso
Laboratory for Hydrospheric Processes, NASA Goddard Space Flight Center, Greenbelt, Maryland

G. F. Cunningham
Jet Propulsion Laboratory, California Institute of Technology, Pasadena

Abstract. By definition, ice which survives the summer is classified as multiyear ice. Thus the area covered by multiyear ice during the winter should be nearly equivalent to the ice area during the previous summer's minima. This condition provides a reasonable criterion for the evaluation of ice concentration and ice type retrieval algorithms using remote-sensing data sets. From special sensor microwave imager (SSM/I) data the NASA Team algorithm estimates the multiyear, first-year, and total ice concentrations during the winter using combinations of the polarization and spectral gradient ratios. The Team algorithm provides only estimates of ice concentration in the summer. From ERS 1 synthetic aperture radar (SAR) data the remarkably stable contrast between multiyear ice and first-year ice in winter provides consistent estimates of multiyear ice concentrations. In the summer, multiyear ice concentration cannot be estimated from SAR or SSM/I data because free water on the surface effectively masks the backscatter and emissivity signature of this ice type. From SAR data a technique which takes advantage of the high backscatter of wind-roughened open water as a discrimination feature is used to estimate the total ice concentration in the summer. With a year-long (January 1992 to January 1993) data set from the Beaufort Sea we found that the multiyear ice concentration estimates from the SAR data are stable and are nearly equivalent to the ice concentration estimated at the end of the previous summer. We contrast this with the variability of the multiyear ice concentration and ice fraction estimates obtained using SSM/I data. The Team algorithm produces ice concentration and multiyear ice estimates which are consistently lower than those from the SAR data. We discuss reasons for these discrepancies and the implications of the higher than previously noted multiyear ice concentrations.

1. Introduction

The total ice and multiyear ice concentrations estimated using the NASA sea ice algorithm [*Cavalieri et al.*, 1984] or Team algorithm provide a fairly long temporal record of the character of the polar ice cover using data from the scanning multichannel microwave radiometer (SMMR) and its successor, the special sensor microwave imager (SSM/I). If these seasonal records are examined, one finds that the retrieval algorithm provides estimates of multiyear ice concentration in the winter which are much lower (by up to 30%) than that of the total ice concentration in the summer. From an ice balance perspective, such large discrepancies need to be resolved. If ice which survives the summer is classified as multiyear ice, then the multiyear ice concentration during the winter should be nearly equivalent to the ice concentration during the previous summer's minima, differing by an amount due to melt, ridging, new/young ice formation, and export of ice from the Arctic. This mismatch was noted by a number of investigators from the point of view of this variability of the multichannel microwave signatures of sea ice on regional studies [*Thomas*, 1993], from comparison with surface measurements [*Grenfell and Lohanick*, 1985; *Grenfell*, 1992], and from an ice balance perspective [*Comiso*, 1990; *Rothrock and Thomas*, 1990; *Thomas and Rothrock*, 1993].

Passive microwave algorithms used for ice parameter retrievals are summarized by *Steffen et al.* [1992]. Currently, the Team algorithm's estimates provide a long-term record of the characteristics of the sea ice cover. The only other estimate we are aware of [*Wittmann and Schule*, 1966] gives a multiyear ice concentration of over 70%, which was based on aerial surveys. It is apparent that more accurate multiyear ice estimates are needed to establish the true nature of the ice cover. Validation studies for the Team algorithm show overestimates in some areas and underestimates in others [*Cavalieri*, 1992]. *Rothrock and Thomas* [1990] used a Kalman filter/smoother to couple a physical model and the Team algorithm analyses to obtain optimal estimates of the total ice and multiyear ice concentrations to overcome the inconsistencies in the temporal record. The Kalman filter increases the winter multiyear ice concen-

Paper number 96JC02455.
0148-0227/96/96JC-02455$09.00

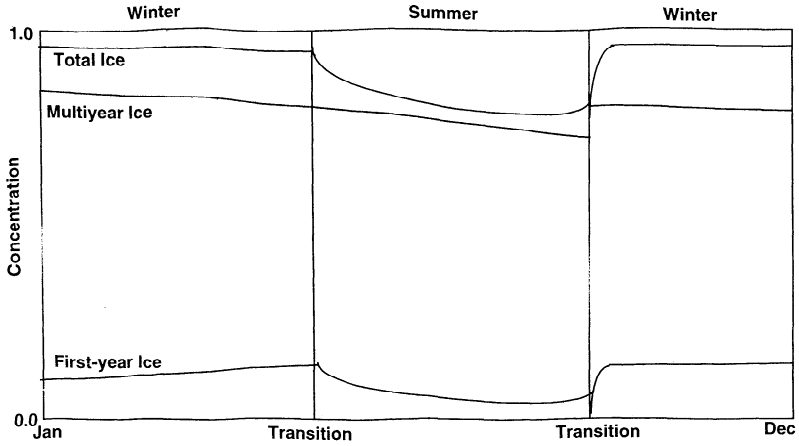

Figure 1. Expected variability of sea ice cover over an annual cycle.

tration and decreases the summer ice concentration to reduce the inconsistency between the summer and winter concentration estimates from the Team algorithm. So although this consistency condition is met, they recognized that the filtered estimates would be biased if the measurements are themselves biased. They also demonstrated that the assumption of pure signatures introduces biases in the Team algorithm estimates.

With the launch of the European Earth Remote Sensing Satellite (ERS 1) in July of 1991, this C band synthetic aperture radar (SAR) has provided an alternate view of the ice cover than that offered by the SSM/I sensor. The much higher resolution allows us to distinguish between floes and leads most of the time, and there is sufficient backscatter contrast between the principal ice types to allow their identification under certain conditions (discussed more later). The limitations of sensor swath width (100 km), orbit orientation, and lack of an onboard tape recorder, however, did not provide a system suitable for routine large-scale monitoring of the Arctic sea ice cover in the SSM/I fashion. Here we compare the ice concentrations derived from a set of SAR data and the ice concentrations estimated using the Team algorithm. The questions we would like to ask are (1) how do the average total and multiyear ice concentrations vary over a seasonal cycle and (2) what are the accuracy and precision of the estimates from active and passive microwave data? A comparative study of results from SSM/I and SAR data is made here to gain insight into answers to these questions.

As a basis for evaluation of the retrieval algorithms we would like to present a simplified view of the expected character of the annual cycle of the Arctic sea ice cover (Figure 1). The validity of the estimates of the total and multiyear ice concentration obtained using the Team and SAR algorithms is measured against these trends. In the winter the areal extent of multiyear ice remains fairly constant with a decreasing trend due to ridging and export of ice principally through the Fram Strait. The total ice concentration stays close to unity because water in open leads freezes rapidly at subfreezing temperatures. The first-year ice concentration increases as the ice in previously open leads thickens and is able to survive the mechanical stresses within the ice cover. After the spring/summer transition the total ice, multiyear, and first-year ice concentrations would start to decrease due to lateral melt because of the above-freezing air temperatures throughout most of the Arctic. Very little first-year ice is produced during the summer. All of the ice, including first-year ice, from the previous winter which survived the summer season becomes multiyear ice (by definition), resulting in a sharp increase in the multiyear ice concentration. Consequently, the multiyear ice concentration at this time should be roughly equivalent to the ice concentration at the summer's minima. This cycle is then repeated during the next ice season. We note here that the schematic in Figure 1 is more valid as a regional view rather than a large-scale view. On the Arctic scale the seasonal transitions occur at different dates at different locations and the transitions themselves are not as sharp as the view presented here.

In this study we present results of a comparative analysis of the multiyear ice concentration estimates from the Team algorithm and the SAR retrieval algorithm using a data set spanning January 1992 through January 1993. We also compare total ice concentrations and discuss the differences in the three periods separated by the onset of melt during the spring/summer transition and the fall freeze-up during the summer/winter transition. The differences are examined in terms of consistency in the analysis and the effect of signature variability on these estimates. The implications of these differences on the multiyear ice balance and computation of the actual ice concentration are discussed.

2. Data Description

Region of Study

The region we selected for the comparison is shown in Figure 2. The shape of the eastern and western boundaries of the region is defined by ERS 1 orbits used in this study. The southern boundary is at approximately 70°N with the northern boundary at approximately 84°N. This covers an area of approximately 1500 km by 900 km. The region is selected because this is an area known to have relatively high multiyear ice concentration. Also, the data set is readily available to us, at the time of this study, through the Alaska SAR Facility.

SSM/I Data

Brightness temperatures from all SSM/I channels were gridded to a standard rectangular polar stereographic format for analysis of the dual-polarized multispectral data. Daily averages were mapped to a 304 by 448 matrix with a grid size of 25 km by 25 km. The 19- and 37-GHz channels were used in the retrieval of total and multiyear ice concentrations, and the 22-GHz channel was used to provide an ocean mask. The

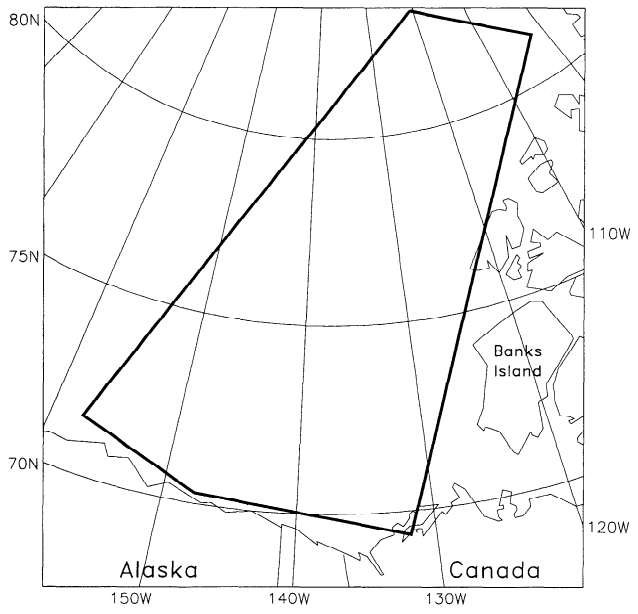

Figure 2. The comparative analysis uses ERS 1 SAR data and SSM/I data from the region defined by these boundaries.

radiometer observations were made at an angle of incidence of 53.1° at the Earth's surface with a swath width of 1394 km.

SAR Data

A total of 571 ERS 1 SAR images between January 1992 and January 1993 were used for this comparative analysis. This represents a sample of approximately 44 images per month. The SAR images for a particular month were collected within a 3-day period early in the month. The ERS 1 SAR is a C band (5.3 GHz) radar operated with vertical transmit and receive polarizations at a look angle close to 20°. The antenna's elevation beam illuminates an across-track swath of approximately 100 km in width. Incidence angles on the ground vary between 19° at near range and almost 26° at far range. The image data used in this study were received and processed at the Alaska SAR Facility (ASF) in Fairbanks, Alaska. Each image frame covers an area of approximately 100 km by 100 km. The image data used in this study have sample spacings of 100 m (created from spatially averaging four-look, 25-m resolution data). This lower-resolution data type, with approximately 40 looks, was selected because of lower speckle content. This reduces the uncertainty in the data analysis. Ancillary data are provided with each image frame for calibration and conversion of the 8-bit digital data into normalized backscatter cross-sections.

The SAR analysis algorithms we use require a calibrated data set because the identification of the sea ice types is based on tabulated expectations of their respective backscatter [*Kwok et al.*, 1992]. Calibration of the radar is measured in an absolute and relative sense. The absolute calibration accuracy metric quantifies the uncertainty in the observed normalized backscatter cross-section (σ_O) measurement relative to the actual σ_O of a distributed target. Typically, this appears as a bias when an identical target from two image frames (imaged at different times) is compared. The in-scene variance of a radar target known to have uniform backscatter cross section is measured by the relative calibration accuracy of the data. Relative calibration of the radar is usually better than the absolute calibration and is easily maintainable especially if the radar sensor is stable. The data products used in this study have expected absolute and relative accuracies of 2 dB and 1 dB, respectively.

Wind and Temperature Fields

Surface wind and temperature fields obtained from the National Meteorological Center (NMC) were gridded to a 2.5° latitude by 5° longitude grid at twice-daily intervals centered at 0000 and 1200 UT. In the NMC analysis process the observations are interpolated to a grid. Because large parts of the world have no observations and the data are not taken at one time (observations are included if they are within 6 hours of the forecast time), NMC uses a model forecast to help with the interpolation. Therefore the data provided are a blend of sparse observational and model data. While the temperature fields may not represent the actual near-surface air temperature due to uncertainty in the NMC analyses, the temperature fields are biased due to difficulty in modeling the inversion layer. We use these air temperature fields as coarse indicators of whether the air temperature is below −10°C to ensure stability of the sea ice signatures. Above approximately −10°C the metamorphosis of the constituents of the ice volume would alter the scattering response of all ice types.

3. Data Analysis

We describe the algorithms used in our analysis and their expected precision. Precision is used here as a measure of the repeatability of these estimates rather than an indicator of absolute accuracy. We do not have independent measurements of the true multiyear and ice concentrations for assessing the accuracy. The details of the Team algorithm have been discussed in the references provided below. Here we provide a more detailed accounting of the SAR algorithms since they are relatively recent developments and have not been characterized as extensively as the passive microwave algorithms. The variability of the passive and active sea ice signatures is typically affected by surface conditions. In the remote sensing of the ice types we would ideally like the ice layer rather than the surface cover (e.g., snow) to provide the largest contribution to the observed signature such that the retrieval algorithms are not confounded by surface effects. This requirement is not always satisfied. These algorithms are also dependent on the spatial and temporal stability of the signature of ice types for efficient interpretation of the active and passive microwave data. Otherwise, overlapping and varying brightness temperature and backscatter signatures are difficult for simple classification schemes. We also note that in the consideration of active and passive microwave measurements, surface processes typically have a larger effect on the shorter wavelength observations and lower frequencies are less affected by the atmosphere and minor modifications of the snow layer.

Total/Multiyear Ice Concentrations From SSM/I Data

Gridded brightness temperatures from all SSM/I channels are used as inputs to the retrieval procedures. Using the spectral gradient ratio (GR) at 37 GHz and 19 GHz and the polarization ratio (PR) at 19 GHz, the concentrations of open water, first-year ice, and multiyear ice are computed at each 25-km cell using the NASA Team algorithm [*Cavalieri et al.*, 1984; *Gloersen and Cavalieri*, 1986]. The procedure to estimate the total ice and ice type concentrations in an SSM/I pixel is based on a mixing formulation which assumes that multiyear

Table 1. Consistency in the Classification of Multiyear (MY) Ice in 3-Day Repeat ERS 1 SAR Imagery

Image Pair	MY Concentration
3620, 4029	98.35, 98.29
3621, 4093	97.65, 97.84
11280, 11995	95.83, 96.16
11284, 11959	96.35, 96.37
11287, 11962	95.79, 95.83
11288, 11963	94.74, 94.56
11289, 11964	94.89, 94.61
11295, 11970	70.51, 70.32
13009, 13726	95.32, 95.96
13011, 13728	94.26, 94.34
Rms difference	0.27

ice, first-year ice, and open water have temporally and spatially stable signatures, i.e., GRs and PRs. *Cavalieri et al.* [1984] recognized the importance of selecting tie points to tune the algorithm for local differences in ice emissivities; however, a single set of "global" tie points are currently used to calculate ice concentrations. The precision of the open water estimates, in the Beaufort and Chukchi Seas, ranges between $-2.1 \pm 3.1\%$ and $0.6 \pm 7.4\%$ [*Cavalieri*, 1992]. The variance in the multiyear ice estimates, when compared with estimates from other sensors, is higher and trends are not evident. The reader is referred to *Cavalieri* [1992] for a summary of the differences between the Team algorithm ice concentrations and those derived by other sensors. As part of the SSM/I validation program in March 1988 [*Cavalieri et al.*, 1991], coincident measurements of the sea ice were made with the Jet Propulsion Laboratory (JPL) C band SAR and the Goddard Space Flight Center (GSFC) aircraft multifrequency microwave radiometers (AMMR). Differences between multiyear ice concentrations estimated from the JPL C band SAR imagery and from the GSFC AMMR radiances using an SSM/I type algorithm show that the AMMR concentrations are smaller on average by $6\% \pm 14\%$.

Total/Multiyear Concentrations From ERS 1 SAR Data in Winter

In the winter we use a fairly simple backscatter-based classification scheme [*Kwok et al.*, 1992] to classify each SAR pixel into one of the three types: multiyear, first-year, and open water. No attempt is made to resolve the different types within a pixel. The persistent backscatter contrast between multiyear ice and first-year ice [*Kwok and Cunningham*, 1994a] was used to discriminate between the two ice types. An example of an ice classification map is shown in Plate 1. *Fetterer et al.* [1994] assessed the performance of this algorithm and reported that the precision of multiyear ice concentration estimates is better than 6% and that first-year ice was easily separated from multiyear ice. *Steffen and Heinrichs* [1994] also pointed out that first-year ice and old ice could be clearly separated based on their scattering coefficients; their comparative study with Landsat data showed an error of 5–8% for compact ice conditions. Both studies indicated that the algorithm sometimes fails to correctly classify open water and new ice due to overlap in the backscatter distributions of the ice types. As an independent estimate we evaluated the precision of our multiyear ice retrieval procedure using 10 pairs of SAR images from the same geographic location acquired during the 3-day repeat phase of the ERS 1 mission. The differences are less than 1% (Table 1). The results suggest that the signatures used in the classification process are stable at least over the short term and that the higher uncertainty observed by *Fetterer et al.* [1994] is probably due to a combination of spatial or temporal variability of the ice signature over the longer term. The higher than normal backscatter of frost-flower-covered sea ice could also be problematic due to their time-dependent signature [*Kwok and Cunningham*, 1994b], but we expect the fraction of this ice category to be less than the fraction of newly frozen leads, which is less than a few percent in the winter Arctic away from the coast. Another limitation with this backscatter-based classification is the potential confusion between deformed first-year ice and multiyear ice especially in the region of transition between the seasonal and perennial ice zones [*Rignot and Drinkwater*, 1994]. Both ice types have similar backscatter, and on the basis of their analysis of aircraft SAR data the multiyear ice concentration could be overestimated by as much as 15%. There is also the issue of flooding and refreezing which suppress the backscatter from the ice volume and cause underestimates in the multiyear ice concentration. In the next section we address these issues in more detail.

Ice Concentration From ERS 1 SAR Data in Summer

We do not estimate the multiyear ice concentration in the summer. After the onset of melt in the spring the free water in the snow layer or bare ice surface acts as a barrier to radar penetration into the multiyear ice layer, thus reducing the volume scattering contribution to the observed backscatter. The contrast between first-year and multiyear ice at C band (see difference between Figures 3e and 3f) is lost and there is at present no effective means for ice type classification in the summer time. The summer sea ice cover at C band has an average range of backscatter that is between -17 and -12 dB. At C band vertical transmit and receive polarizations (C-VV), open water backscatter is dependent on wind speed and is typically higher than that of the ice cover if the wind speed is above 4–5 m/s. The azimuthal look direction introduces only 1–2 dB of modulation of the backscatter at ERS 1 look angles. We estimate open water in leads by using an algorithm [*Comiso and Kwok*, this issue] which takes advantage of the higher backscatter of wind-roughened open water relative to the ice cover. With an indication of wind speed the thresholds are adjusted visually to discriminate between water and ice. The precision of our ice concentration estimates is approximately 2–3% during windy conditions (above 4–5 m/s). During calm conditions, ice concentrations are also derived, but the uncertainties are higher because of the decrease in contrast. The precision of these measurements, based on repeated visual classification of these images, is approximately 10%. We avoid classification of certain images which lack sufficient contrast between ice and open water. We show an example to illustrate the effectiveness of this technique. Plate 2a shows a typical summer SAR image near the ice edge, while Plate 2b shows a color-coded version of the result obtained using this classification procedure. Since melt ponds are blended in with the backscatter of ice and snow on ice floes, the melt ponds are classified as sea ice in our algorithm.

Subresolution leads are not accounted for and contribute to an overestimation of the ice concentration. There does not exist in the observational literature the fraction of leads that are not resolved by the SAR data used in this analysis. R. Lindsay (personal communication, 1995) studied the problem using Channel 3 of an April Landsat Thematic Mapper (TM) image from the Beaufort Sea. His results show that approxi-

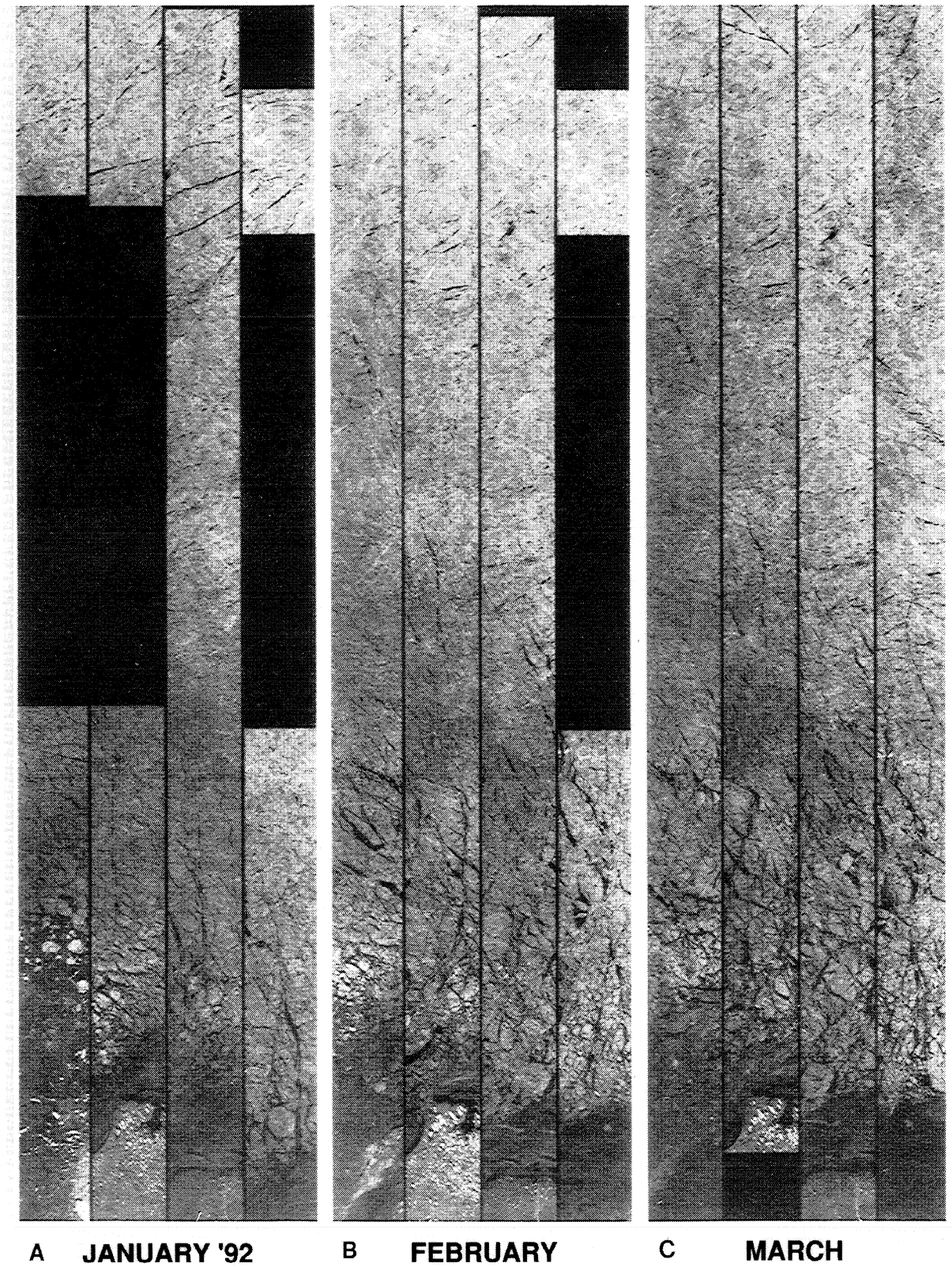

Figure 3. View of the ice cover from SAR: (a) January, (b) February, (c) March, (d) April, (e) May, (f) June, (g) July, (h) August, (i) September, (j) October, (k) November, and (l) December. The winter scenes show very stable SAR backscatter while the contrast that is typical in the winter is lost in the summer. The strips are 100 km in width and the longest strips contain up to 15 image frames (or 1500 km in length). (ERS 1 images © ESA 1994)

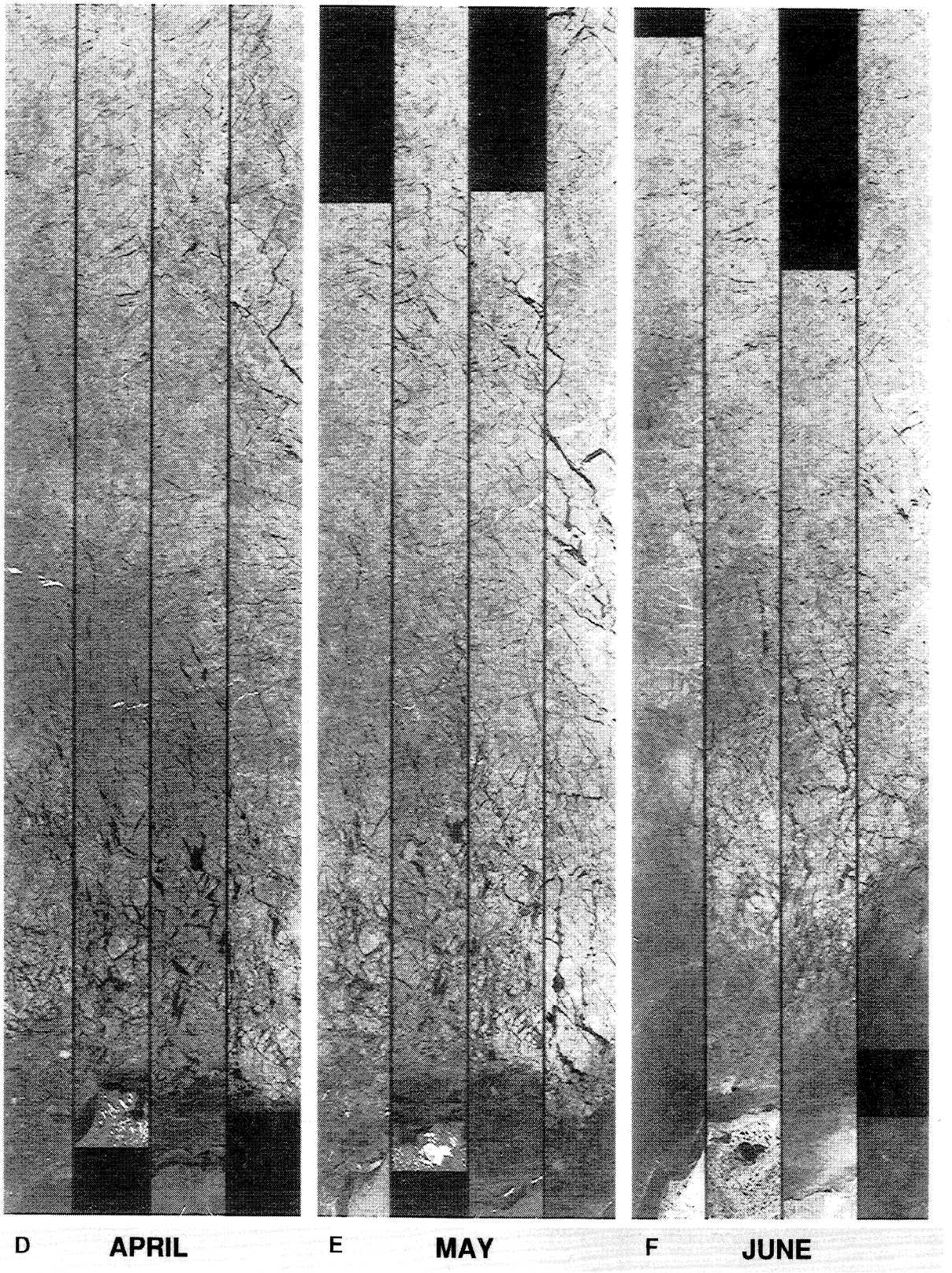

Figure 3. (continued)

mately 22% of the leads have widths less than 100 m. Within that image the mean lead width is 140 m with few leads more than 500 m wide. If these statistics can be regarded as typical for the summer and winter, then in regions with 90% ice cover this resolution problem would cause a 2% error (i.e., 22% of the 10% area occupied by leads) in the ice concentration. More extensive observations, preferably airborne surveys, are necessary to better quantify this error.

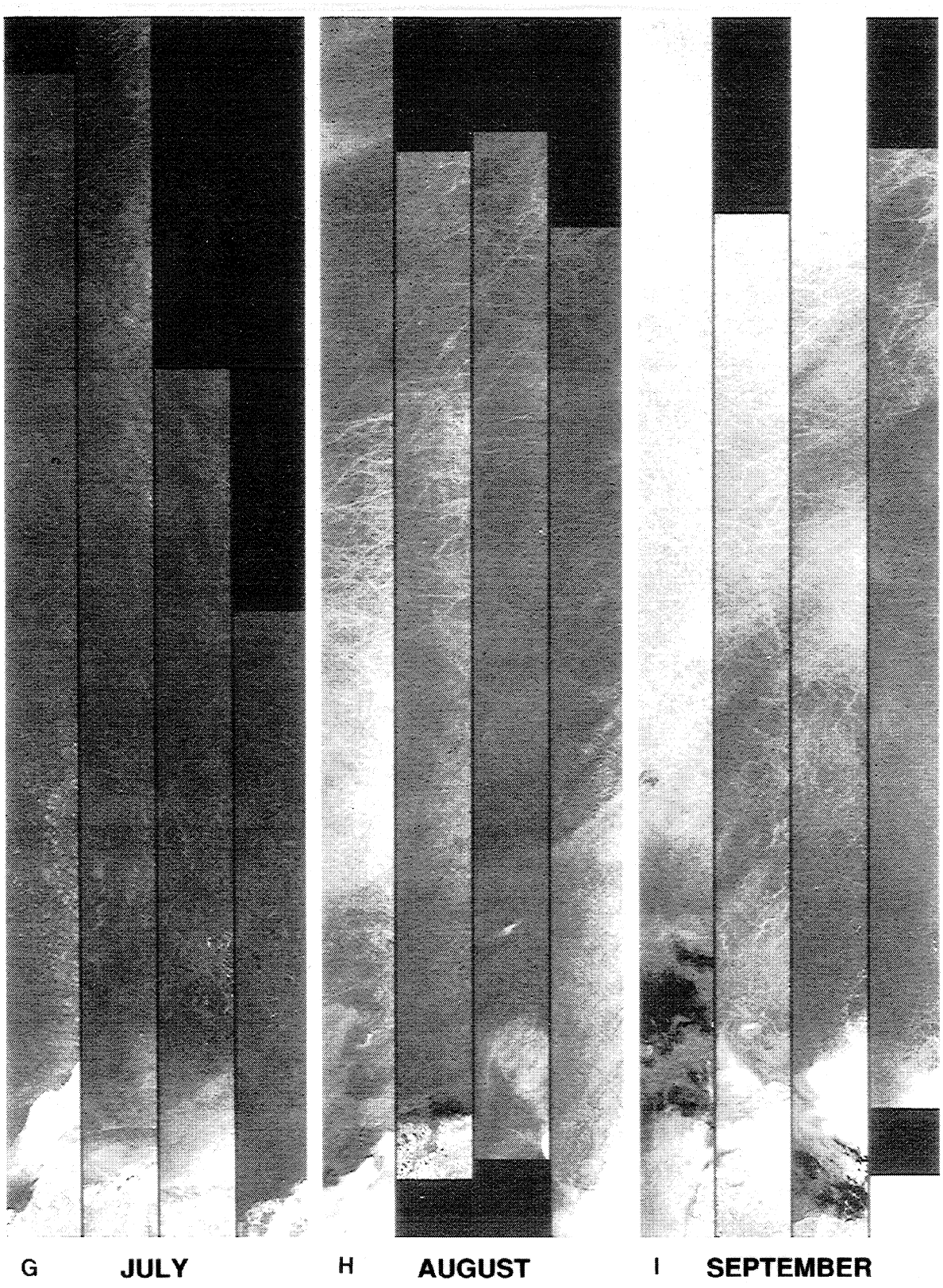

Figure 3. (continued)

4. Results and Discussion

For a quantitative comparison of the estimates from SSM/I and SAR, we divide the area into five latitude bands with intervals of 2.5° starting at 70°N. The images covering the region shown in Figure 2 were analyzed using the SAR algorithms. Coincident SSM/I data at these times and locations were also analyzed. The SAR images for each month over the

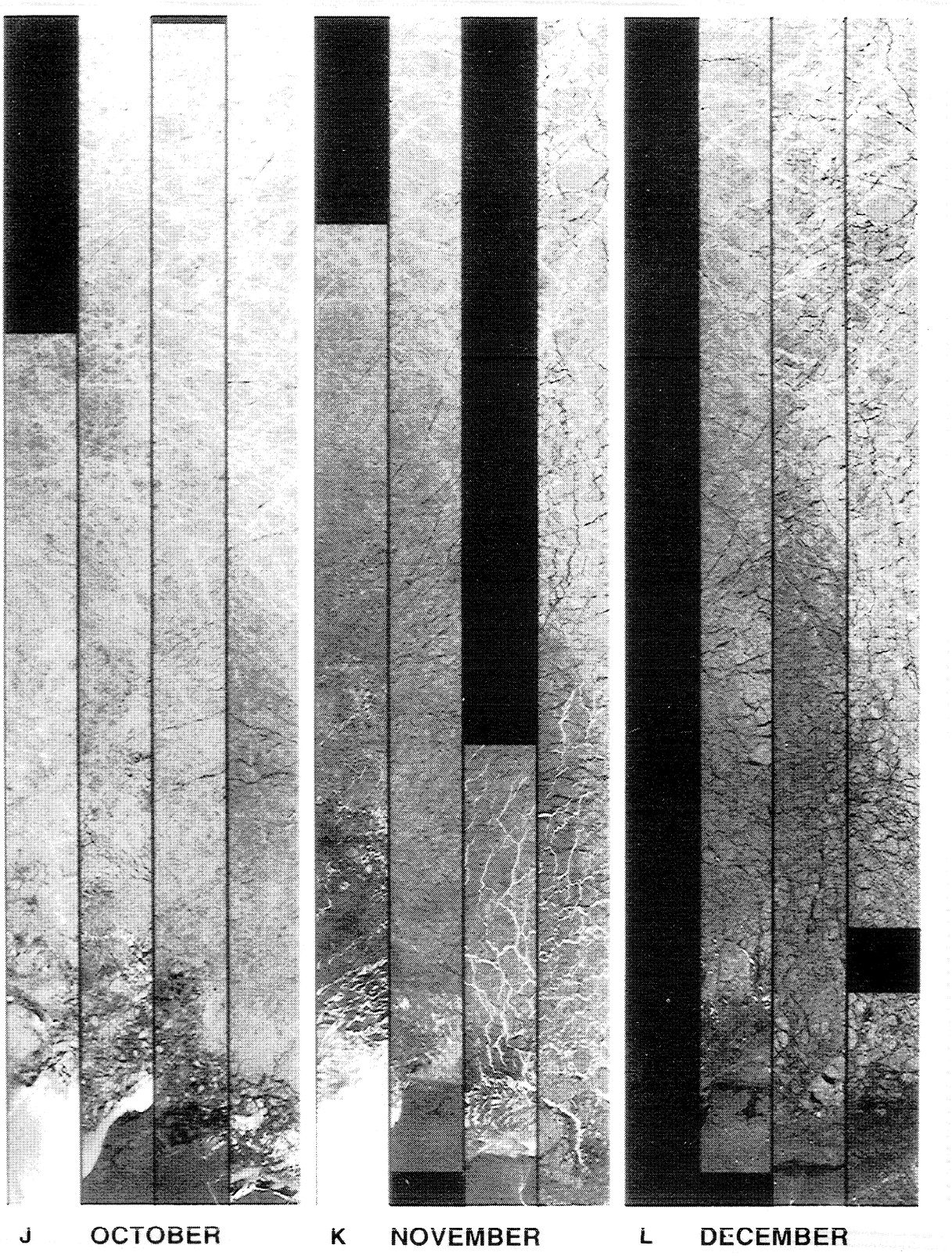

Figure 3. (continued)

region of study are shown in Figure 3. These images show spatial and temporal details about the ice cover and indicate stability in the backscatter distribution, especially in the winter. The ice type and concentration estimates are plotted in Figure 4. The ice concentration results from both procedures were generally consistent except during the summer, while the multiyear ice concentrations differ substantially. A detailed discussion of the results is presented in the following sections.

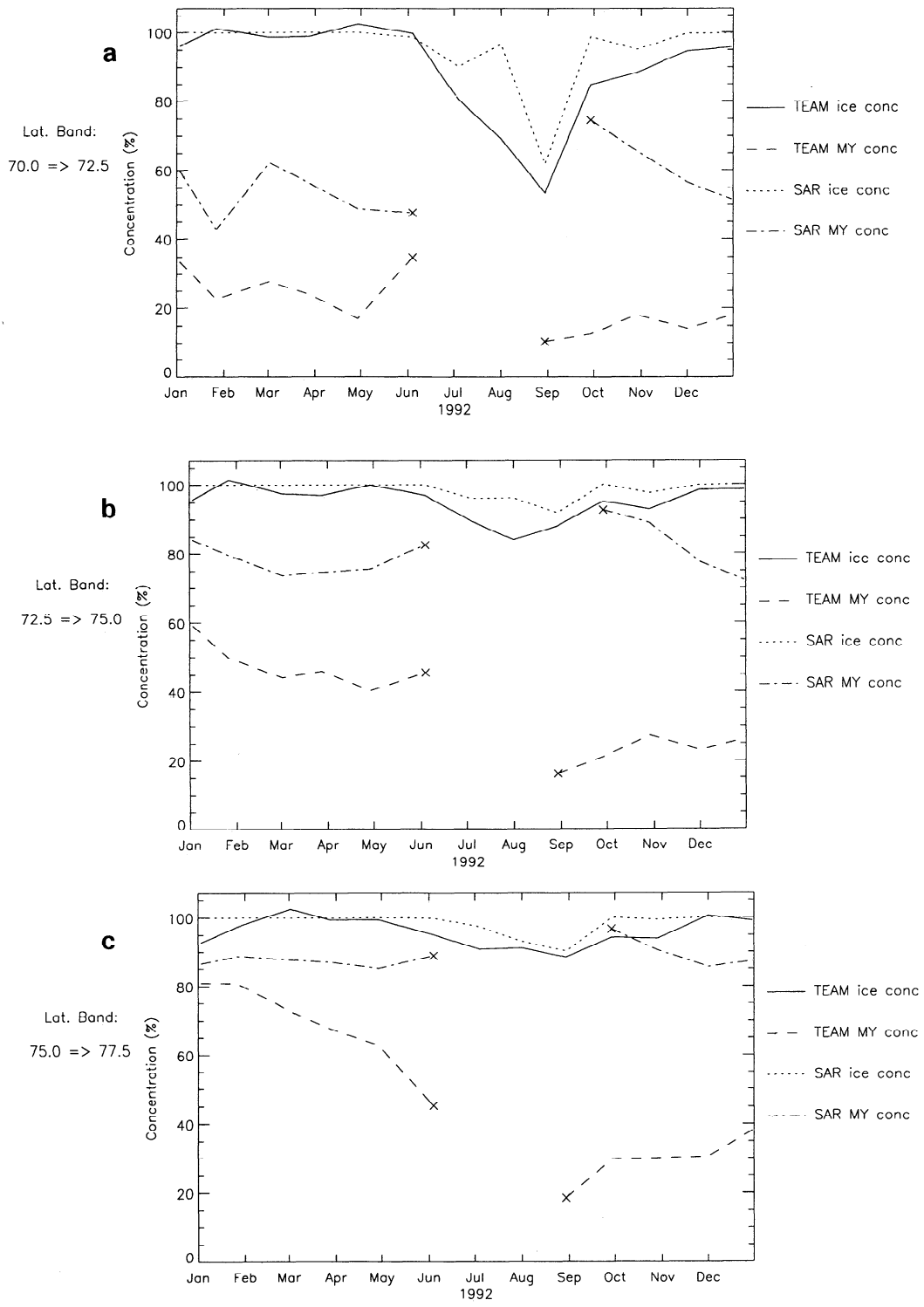

Figure 4. Comparisons of the total ice and multiyear (MY) ice concentrations at five latitude bands: (a) 70.0°–72.5°, (b) 72.5°–75.0°, (c) 75.0°–77.5°, (d) 77.5°–80.0°, and (e) above 80.0°.

Total/Multiyear Ice Concentration (January–May)

In the winter the total ice concentrations from both SSM/I and SAR data sets agree to within the uncertainty of the estimates at all latitude bands. The Beaufort Sea is almost 100% ice covered. We note that the Team algorithm occasionally provides anomalous estimates of ice concentrations that are greater than 100% during the winter when data points lie outside the region of validity in PR and GR space. This is due to variability in ice type signatures, system errors, or weather effects. The estimates are, however, constrained to be less than or equal to 100% in the data products.

The multiyear ice concentrations from the two sensors, however, are quite different. During this period the SAR-derived multiyear ice concentrations are quite stable at the higher latitudes and the variability is within the precision of the algorithm. There is no significant increase or decrease in the amount of multiyear ice except near the transition between the perennial pack and the seasonal ice zone. These multiyear

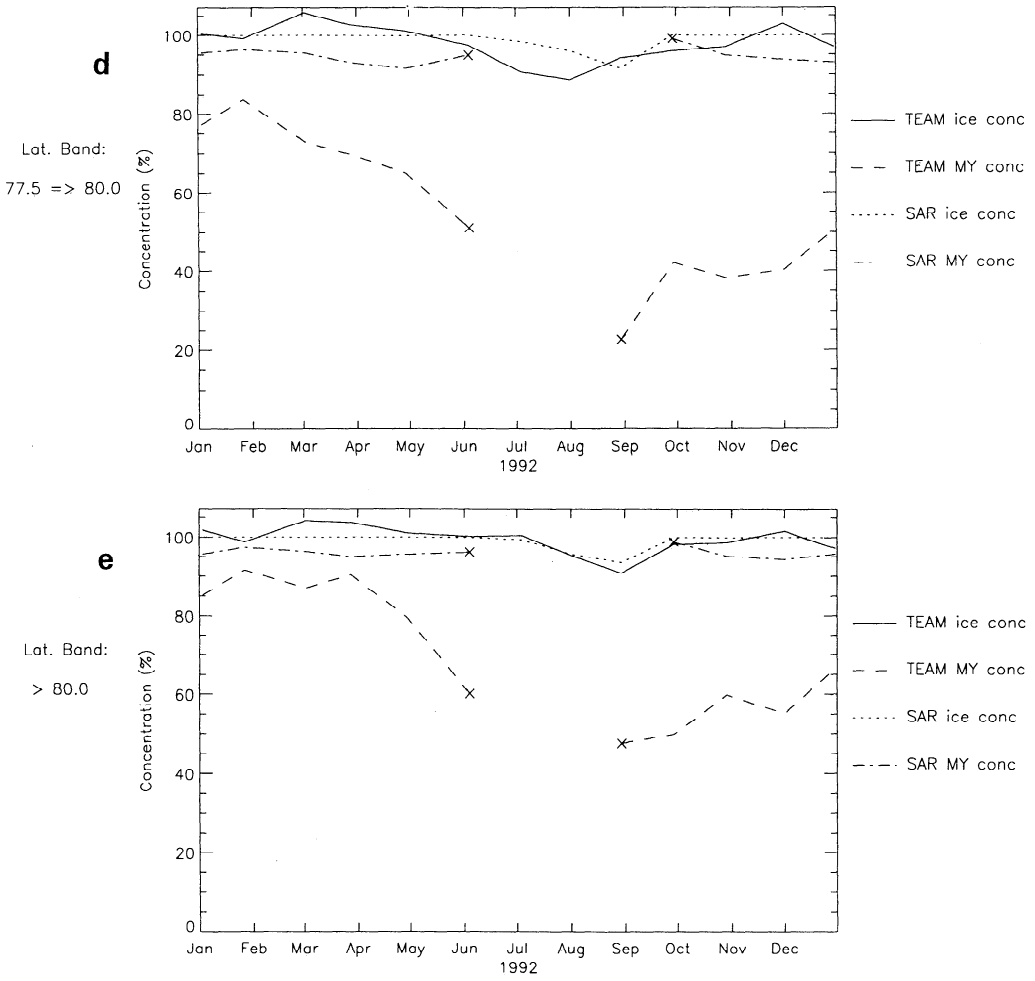

Figure 4. (continued)

concentrations are consistent with ice kinematics (discussed below) during this period and our expectation that this parameter stays fairly constant, especially in this part of the Beaufort Sea and the central Arctic. We attribute the variability in the two lowest latitude bands to the combined effects of ice advection, ridging of first-year ice, and the opening and closing of the ice cover. Sample strips of SAR imagery from this period are shown in Figure 3. The contrast between multiyear ice and undeformed first-year ice persists throughout this period. There are areas of ridged and highly deformed first-year ice which have approximately the same backscatter signature as that of multiyear ice. The SAR-derived multiyear ice concentration isopleths are shown in Figure 5. The patterns of the isopleths have remarkable similarity between observations which are temporally close to each other (e.g., Figures 5a and 5b) and show a north to south decrease in multiyear ice concentration.

The Team algorithm estimates of multiyear ice concentration from SSM/I have substantially different spatial and temporal distributions from those of SAR data (Plate 3). The Team algorithm results as shown in Figure 4 also indicate a trend of decreasing multiyear ice concentration at the higher-latitude bands. For example, between 75°N and 77.5°N, there is a greater than 30% decrease in the multiyear ice concentration between January and May. We check qualitatively to see whether this decrease is consistent with ice kinematics. The ice cover in this region computed from monthly-averaged velocity fields (between September 1, 1991, and April 1, 1992; see Figure 6) is actually slightly convergent (0–10%), which should yield an increase rather that a decrease in the multiyear ice concentration. With a mean velocity of 2 cm/s the total displacement of the ice is less that 240 km, which is small compared to our region, which encompasses an area of 1500 km by 900 km. It is difficult to explain this trend from the perspective of ice cover divergence or a net advection of multiyear ice out of our study region. The SSM/I maps of multiyear ice concentrations of the Arctic Ocean for the months of January and April and their differences are shown in Plate 4. These synoptic maps show a general decrease in multiyear ice between the two observations. We also note that the initiation of this decrease occurs earlier in lower latitudes.

Could the decreasing trend be caused by factors other than ice advection or divergence? To examine this further, we plot (Figure 7) the daily gradient and polarization ratios of three 100 km × 100 km regions centered at the following geographic locations: A (80°N, 130°W), B (77.5°N, 135°W), and C (75°N, 140°W). The gradient ratio is the ratio of the difference between the vertically polarized 19-GHz and 37-GHz brightness temperature measurements and their sum. The polarization ratio is the ratio of the difference and the sum of the vertically and horizontally polarized brightness temperatures at 19 GHz. We draw the reader's attention to the gradient ratio. At high ice concentrations in the winter the gradient ratio is the prin-

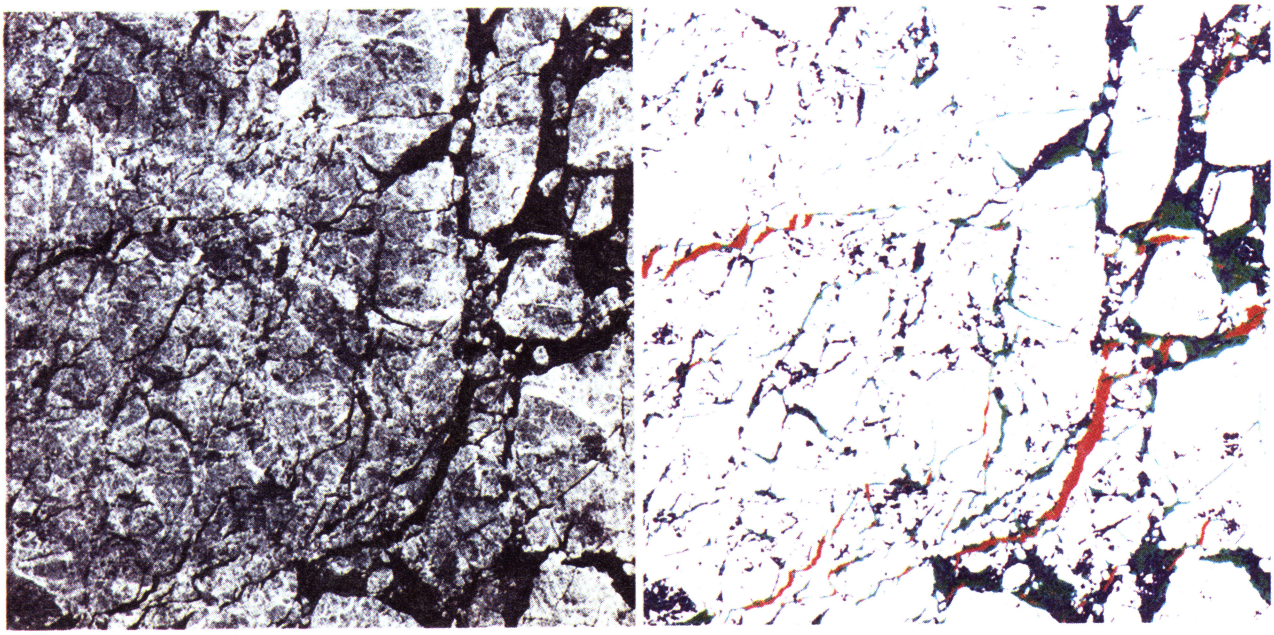

A

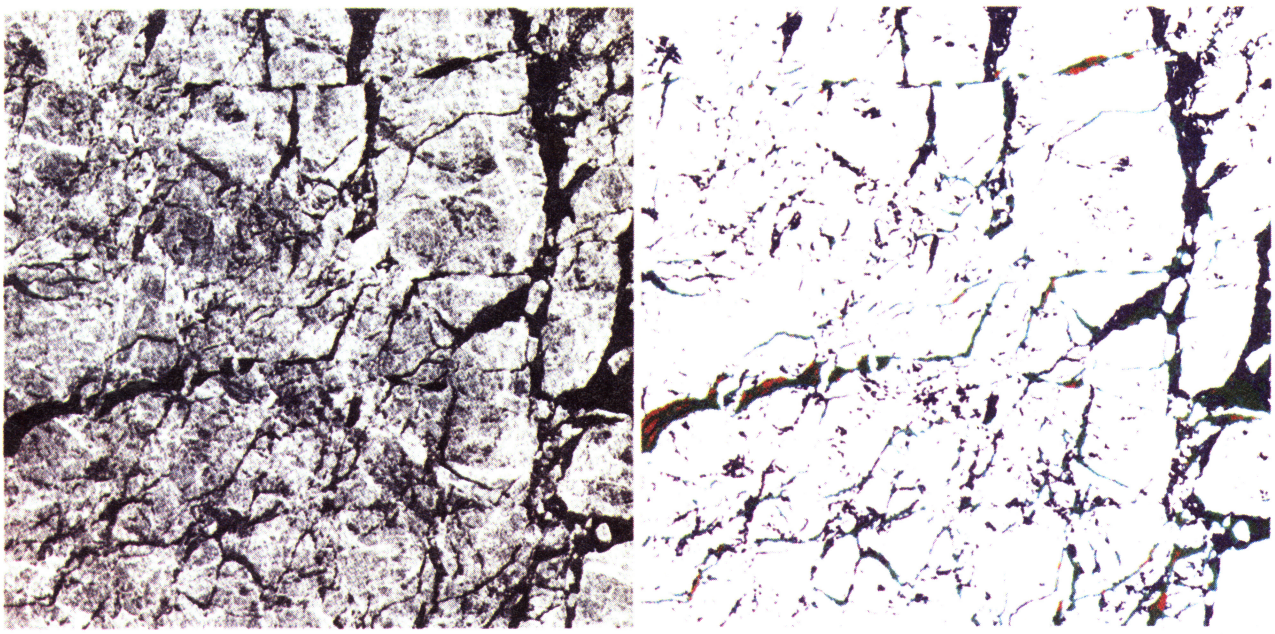

B

Plate 1. Sample SAR ice classification map (winter). (a) The image and the ice type map. (b) The image and the ice type map 3 days before the image in Plate 1a. (White, multiyear ice; blue, deformed first-year ice; green, undeformed first-year ice; red, smooth thin ice or calm open water). (ERS 1 images © ESA 1994)

cipal parameter which allows the separation of multiyear ice from first-year ice. In addition to the small-amplitude variations, there is a slowly increasing trend in this parameter in all three regions and it is especially obvious after day 100. The gradient ratio varies between 0 for 100% first-year ice and −0.09 for 100% multiyear ice. Any increase in this ratio would tend to decrease the estimated multiyear ice concentration. At 100% ice concentration an increase of 0.01 in the gradient ratio would decrease the estimated multiyear ice concentration by approximately 11%. The increasing gradient ratio in the spring (before melt onset) would therefore cause a decrease in the amount of multiyear ice in the region. Because the increasing trend is observed in all three regions, albeit of slightly different amplitude, it would seem to be caused by a large-scale phenomenon. We compute the normalized cross-correlation coefficient of the gradient ratio and polarization ratio time

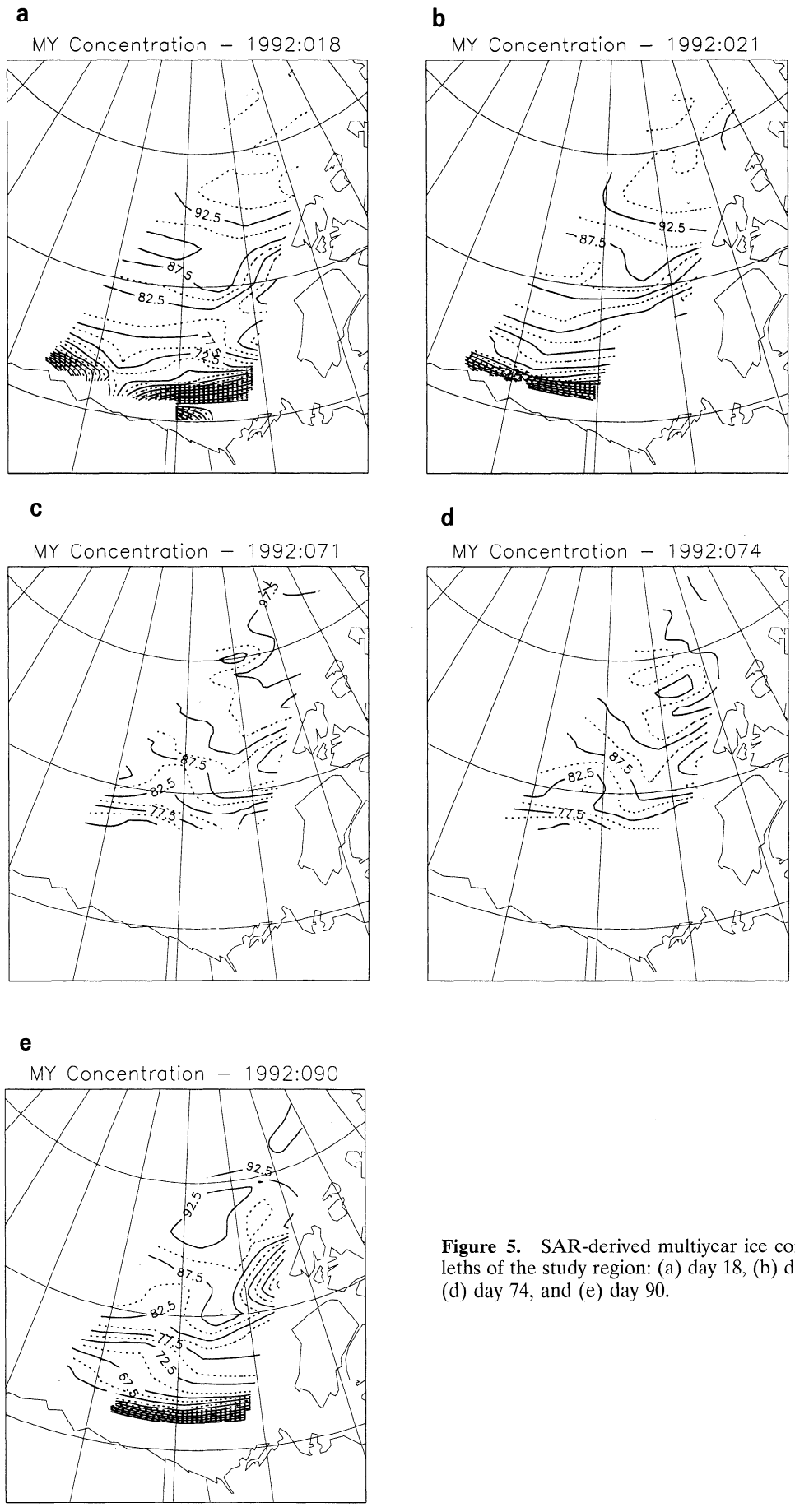

Figure 5. SAR-derived multiyear ice concentration isopleths of the study region: (a) day 18, (b) day 21, (c) day 71, (d) day 74, and (e) day 90.

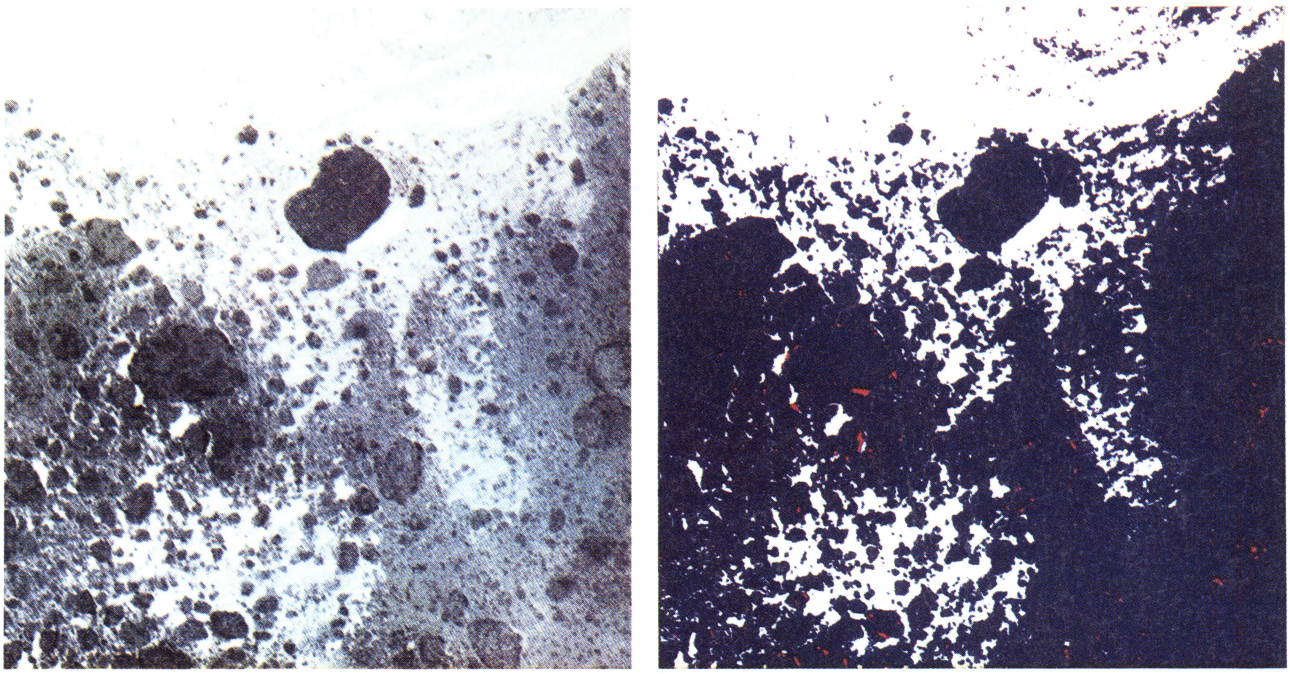

Plate 2. Sample SAR classification map (summer). (a) SAR image. (b) Image classified into ice, grease ice, and open water. (White, open water; blue, ice; red, grease ice). (ERS 1 images © ESA 1994)

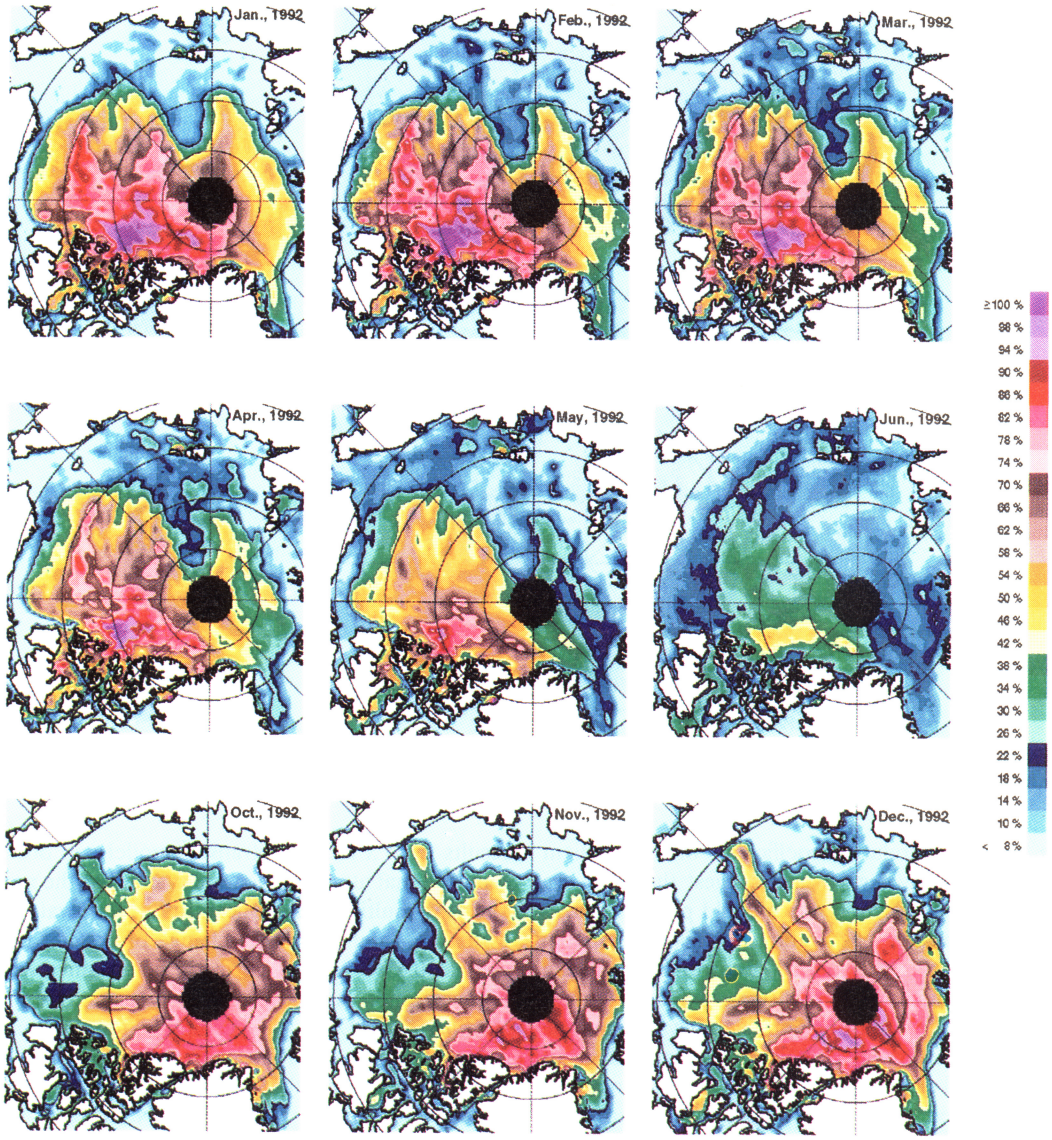

Plate 3. Monthly-averaged SSM/I multiyear ice concentration maps.

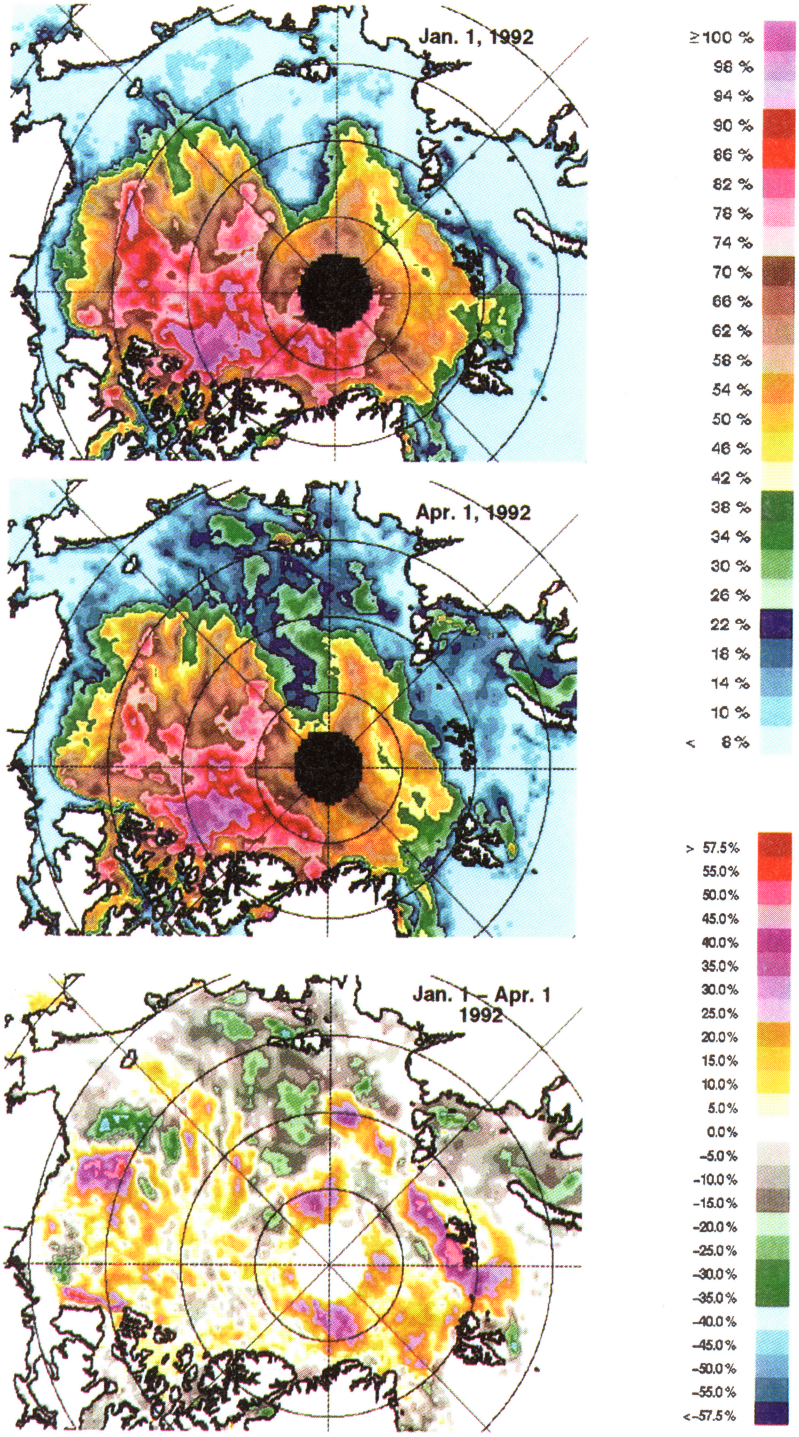

Plate 4. The difference between the Team algorithm-derived multiyear ice concentration on January 1, 1992, and April 1, 1992.

series (Table 2). The correlation coefficients of the gradient ratio time series are fairly high, which suggest that they are covarying with a forcing function which could produce correlated changes in the passive observations at this large spatial scale (500 km). We contrast this to the low correlation between the polarization ratio time series. This suggests that the atmospheric forcing (e.g., water vapor or cloud liquid water) may be the cause of this trend. *Maslanik* [1992] examined the effects of wind, water vapor, and cloud liquid water on ice concentration and ice type calculated from passive microwave data using results from a radiative transfer model and observations. He reported that atmospheric water vapor has the most significant effect on multiyear ice concentration retrieval. In an ice pack with 100% multiyear ice a change of 1 g/cm^2 of water vapor causes 10.8% of multiyear ice to be classified as first-year ice because water vapor causes an increase in the gradient ratio. *Nakamura and Oort* [1988] computed the seasonal water vapor content of the polar atmosphere using station and radiosonde data. They showed that the mean water vapor of the polar atmosphere between 70°N and 90°N increases from less than

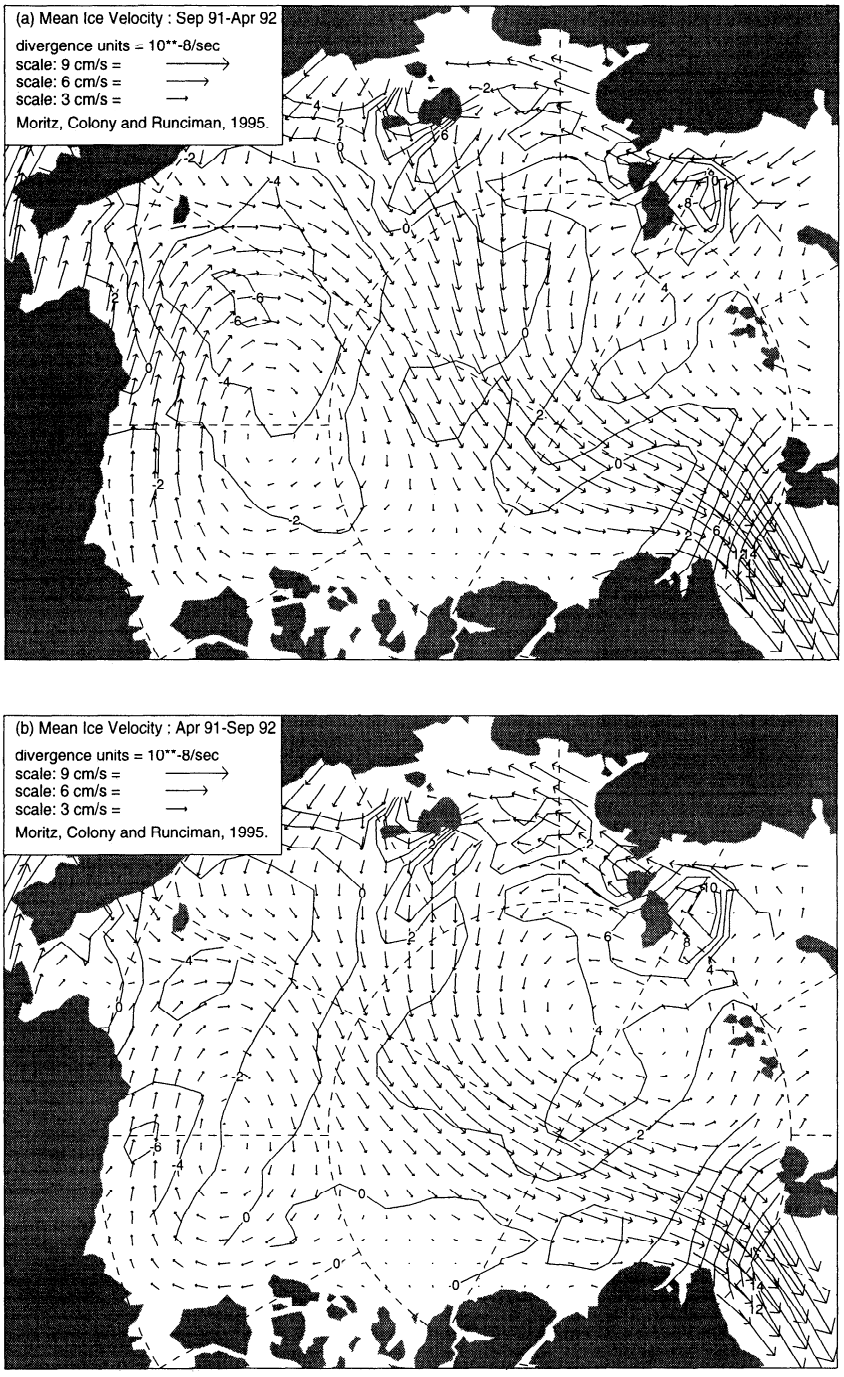

Figure 6. Mean velocity and divergence calculated from wind and buoy data: (a) September 1, 1991, to April 1, 1992; (b) April 1, 1992, to September 1, 1992; (c) September 1, 1992 to April 1, 1993. (Courtesy of R. E. Moritz, R. Colony, and K. Runciman, Polar Science Center, University of Washington)

0.25 g/cm^2 in the winter to more than 1.0 g/cm^2 in the early spring (May). Thus the slowly increasing water vapor content of the atmosphere during the spring could contribute to the decreasing trend in multiyear ice concentration. Conversely, we also note that there is a small decreasing trend in the gradient ratio after fall freeze-up.

The SAR estimates of multiyear ice are higher than those from the Team algorithm at all latitudes. We discuss this below in the context of the character of the ice cover at the end of the summer.

Total Ice Concentration (June–September)

Neither the Team algorithm nor the SAR algorithm provides estimates of multiyear ice in the summer, so only a comparative analysis of total ice concentrations from the two approaches is provided here. *Comiso and Kwok* [this issue] provide a more comprehensive analysis of the differences between active and passive observations for this summer period. After the onset of melt in spring, there is a gradual increase in the areal fraction of open water. The SAR-derived ice concen-

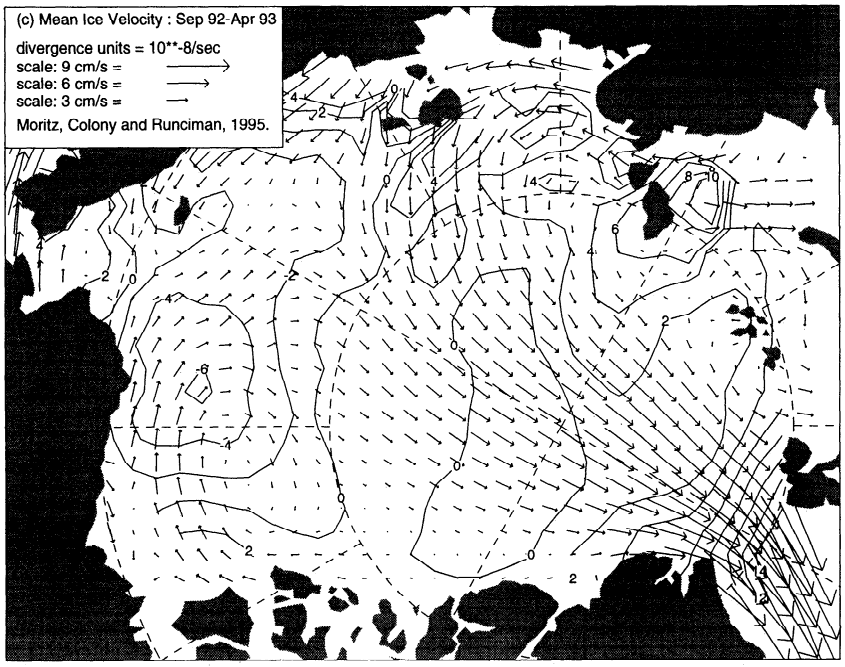

Figure 6. (continued)

trations are typically higher than those of the Team algorithm estimates, and the differences are more pronounced at lower latitudes. A possible cause of this (discussed by *Comiso and Kwok* [this issue]) is the contribution of melt ponds to the open water estimates. Water in melt ponds has the same passive microwave signature as that of water in open leads, causing an underestimation of ice concentration. The larger difference in the lower-latitude bands may be indicative of the latitude dependence of melt pond fraction. We note again that the SAR estimates are biased toward overestimation of ice concentration because subresolution open leads are most likely classified as ice in the summer time. We do not know the relative area contribution of subresolution leads and melt ponds in the summer. If the contribution is small as we discussed earlier, for meltpond concentrations of 20–30% (I. P. Romanov, Morphometric characteristics of ice and snow in the Arctic Basin, unpublished manuscript, 1993) (hereinafter referred to as I. P. Romanov, unpublished manuscript, 1993) the melt ponds would seem to be the dominant factor which affects the microwave signatures. In other words, the underestimation of the Team algorithm is more significant than the bias introduced by small leads. These biases can only be resolved with high-resolution aerial survey.

To gain insight into the discrepancies in the summer ice concentration retrievals, total ice concentration was also derived using the Bootstrap algorithm [*Comiso*, 1995]. A comparison of the two SSM/I results (Plate 5) shows that the Bootstrap algorithm estimates are typically higher than those of the Team algorithm. This is mainly because the tie points used in the Bootstrap algorithm are adjusted to account for changes in surface emissivity during spring, midsummer, and early autumn. However, this procedure is similarly confounded by melt ponds and values are still lower than those of SAR.

Total/Multiyear Ice Concentration (September–December)

At the end of the summer the surviving ice from the previous spring becomes multiyear ice. The SAR results show that the multiyear ice concentration in early October is roughly equivalent to the SAR-derived ice concentration at summer's end. On the basis of the SAR analysis the ice cover seems to be fairly compact with high concentrations of multiyear ice at all latitude bands. In the following months the concentration decreases (especially at the lower latitudes) and returns to a level comparable to that of the previous winter. We attribute this decrease to a convergence in the ice cover in the summer followed by a divergence of the ice cover in November and December. Indeed, the velocity fields (between April 1 and September 1, 1992; see Figure 6) also indicate a convergence of the ice cover in this region of approximately 10–20% in the summer in the lower latitudes and divergence of a smaller magnitude in the fall. The openings in the ice cover in November can be easily observed in the SAR image strips shown in Figure 3. The highly compact ice cover (high ice concentration) can be seen in the images shown in Figures 8a and 8b. At this time the ice cover seems to be composed of primarily multiyear ice with low first-year ice concentration. The high backscatter in the leads is due to wind-roughened open water. In October the ice cover has low first-year ice concentrations, whereas in December the characteristic first-year ice signature (lower backscatter) is more evident due to the thickening of the ice in the open leads created in the previous months. The ice cover attains a backscatter character, in terms of multiyear ice and first-year ice concentrations, that is similar to that of the previous winter (compare Figure 3a and Figure 3l).

There are large differences (about 50%) between the ice concentrations at the end of the summer and the multiyear ice concentration during the subsequent winter as estimated from the Team algorithm. Such a mismatch may be due to the growth of new and young ice during the summer. This would have to occur simultaneously with the melt of a large percentage of multiyear ice. From the time sequence shown in Figure 3 it is difficult to explain how melt and freeze-up of such magnitude could occur in the region. Our expectation is that

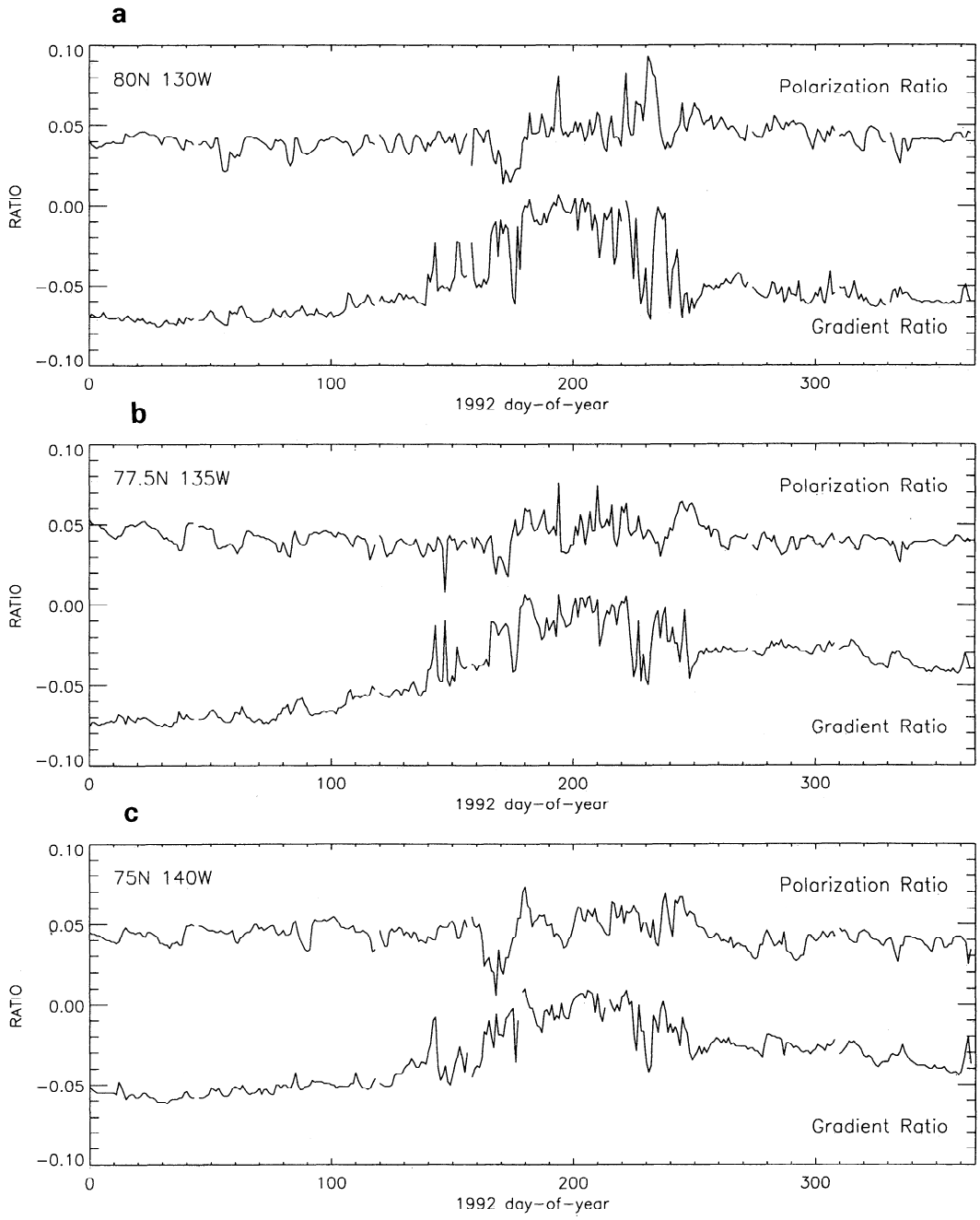

Figure 7. Plots of the daily gradient and polarization ratios centered at three different 100 km by 100 km regions: (a) A (80°N, 130°W); (b) B (77.5°N, 135°W); (c) C (75°N, 140°W).

the amount of multiyear ice could only decrease moderately especially in the higher latitudes in the central Arctic.

Also, there is a large difference between multiyear ice concentration estimates from the SAR and the Team algorithms. The differences are likely due to the spatial variations in the emissivity of sea ice in the Arctic region [*Carsey*, 1982; *Comiso*, 1983]. One factor which causes such spatial changes in the emissivity is melt ponding since frozen melt ponds may have emissivities of first-year ice [*Grenfell*, 1992]. This can be a substantial effect since 20–30% of the summer ice have been observed to be ponded (W. Tucker, private communication, 1994). Another factor could be unusually thick snow cover in some areas that can cause flooding (and subsequent refreez-

Table 2. Correlation Coefficients of the Time Sequences of GR and PR From the Three Regions Centered at A (80°N, 130°W), B (77.5°N, 135°W), and C (75°N, 140°W)

Regions	Correlation
Correlation Coefficients: Gradient Ratios	
A and B	0.83
B and C	0.94
A and C	0.85
Correlation Coefficients: Polarization Ratios	
A and B	0.44
B and C	0.57
A and C	0.21

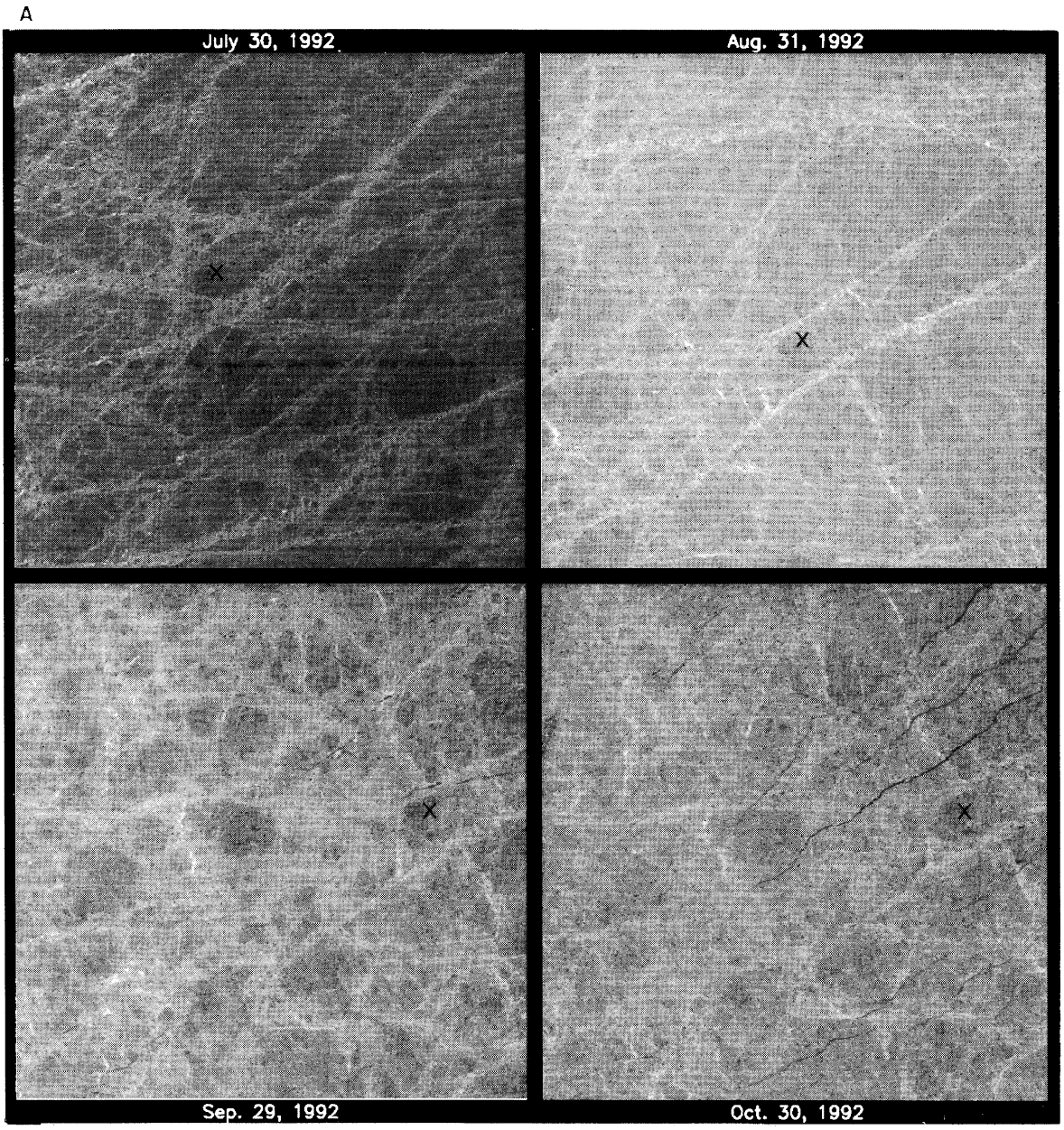

Figure 8. Image sequences showing the compactness of the ice cover before and after fall freeze-up: (a) 80°N; (b) 75°N. The common features between the images (where they could be identified) are marked with crosses. (ERS 1 images © ESA 1994)

ing) at the snow/ice interface. Such effects cause the snow/ice interface to be saline and the emissivity of the ice floe to be similar to that of first-year ice. We note here that after fall freeze-up, the gradient ratios in the three regions (in Figure 7) do not return to their value during the previous year. If the SAR algorithms are correct in estimating the multiyear concentration, the emissivity of multiyear ice after the transition is dramatically different from that during midwinter.

Do the SAR algorithms overestimate multiyear ice concentration? It has been reported [*Rignot and Drinkwater*, 1994] that deformed first-year ice has backscatter characteristics similar to that of multiyear ice in single polarization C band data sets like ERS 1. This would cause the SAR winter algorithm to overestimate the multiyear ice concentration. If this is the case, due to deformation of the ice cover, the amount of deformed ice should increase as the winter wears on, resulting in a gradual increase in the estimated multiyear ice concentration. Indeed, we do not observe such a trend, at least not within the level of uncertainty of the estimates. We discuss the effect of the ridging process with an example. If there is a 15% convergence of the ice cover and this first-year ice area is converted into deformed ice, what is the expected bias in the multiyear ice concentration if the signature of deformed ice is identical to that of multiyear (MY) ice? When first-year (FY) ice ridges, and here we assume that we only ridge the very thin ice from closing of leads, the area is not conserved. The mechanical thickness redistribution takes the volume of ice participating in a ridging event and creates an approximately equivalent volume of ice occupying a smaller area. As a crude estimate, if we use the assumption that all ridged ice is 5 times its original

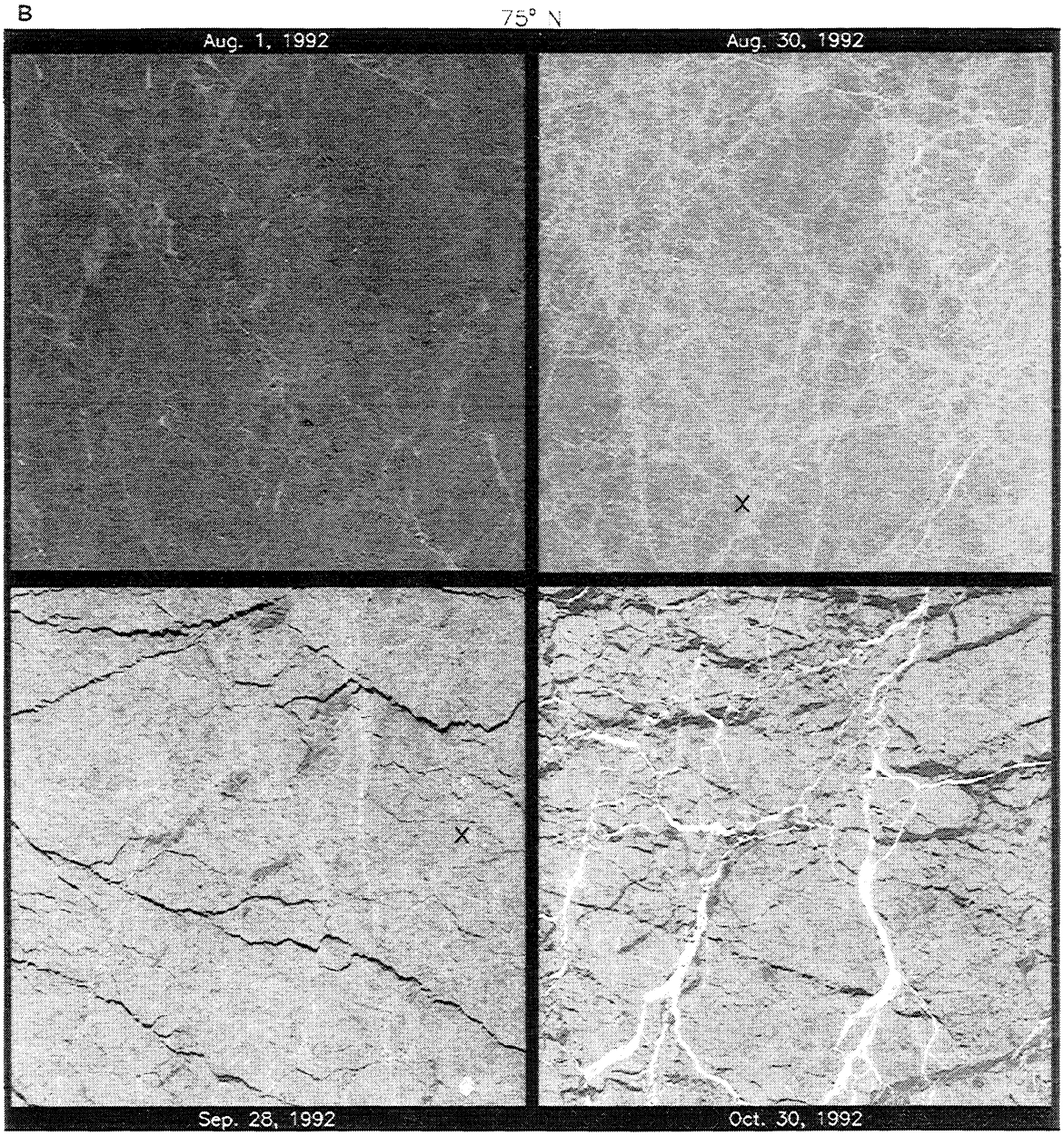

Figure 8. (continued)

thickness before ridging (parameter used by *Thorndike et al.* [1975]), then the contribution of the FY ice area after convergence is much smaller. The 15% undeformed first-year ice area now occupies an area of 3%.

This leads to a very interesting question. If large volumes of first-year ice are piled onto multiyear ice, do we label this area as MY ice or first-year ice? The SAR algorithms described here would label the area as MY. The passive algorithms might label that area differently due to the salinity of the ridged ice. It does not seem to be important from the heat flux point of view because thick ice has a relatively small contribution to the total flux, but it is certainly important from the mass balance point of view. It is possible that deformed first-year ice is piled onto the multiyear ice and therefore does not increase the concentration of multiyear ice even though the polarimetric radar senses a surface type [*Rignot and Drinkwater*, 1994] which seems to be different than that of multiyear ice. We do not know the areal contribution of this deformed first-year/multiyear ice type. If the areal fraction of this surface type is significant, it would affect the passive microwave retrieval results as well.

Comparative Study of the Signatures

The multiyear ice concentrations as inferred from SSM/I data with the Team algorithm make use of gradient and polarization ratios. To gain additional insight into possible causes of disagreements between passive microwave and SAR multiyear ice data, we show scatterplots of the gradient and polarization ratios versus SAR backscatter (in decibels) in Figure 9. Data from the entire Beaufort Sea study area and also from different latitudinal bands indicate that the gradient ratios vary considerably, while the polarization ratios are basically constant for most of the data points. The multiyear ice concentration derived from passive microwave is thus dependent mainly on the gradient ratios.

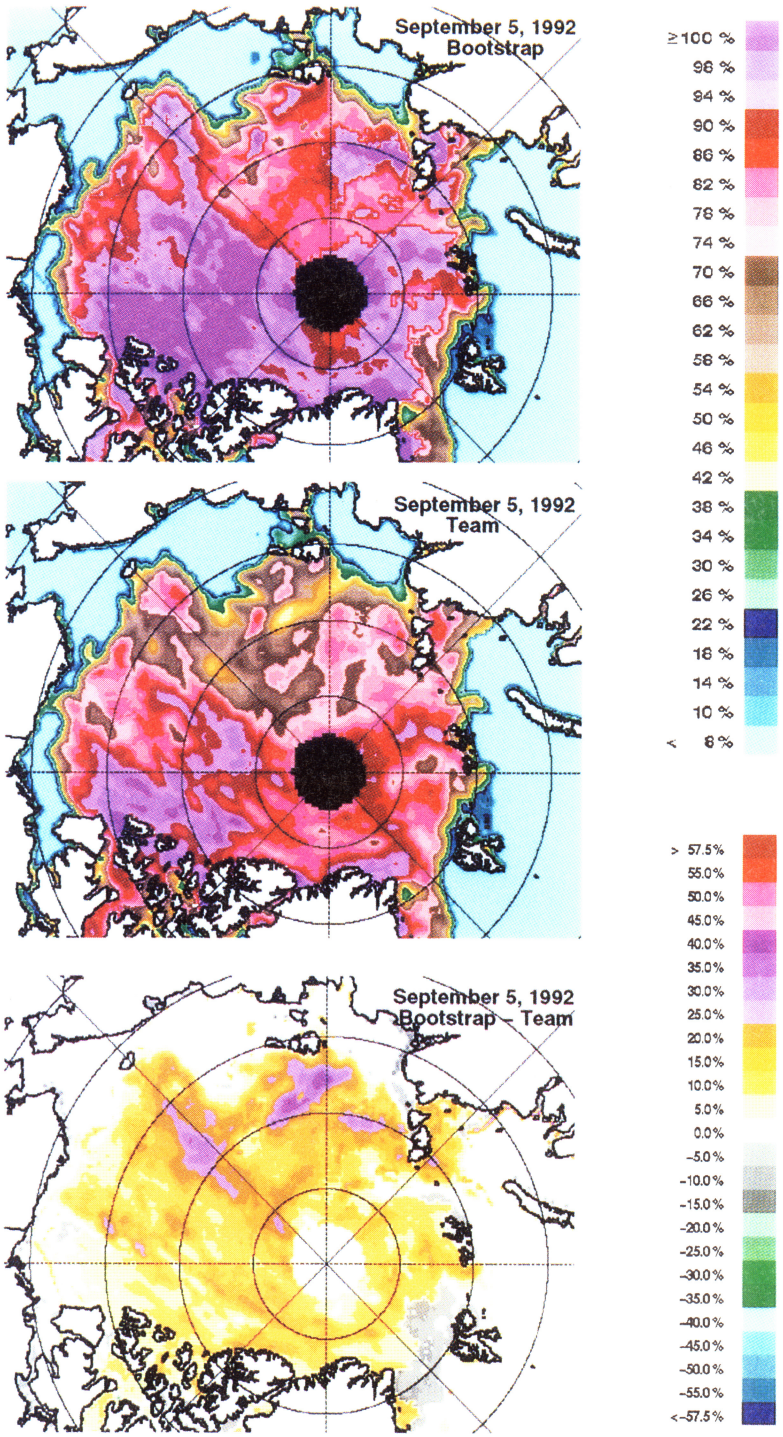

Plate 5. Differences between the Bootstrap and Team algorithm-derived total ice concentration on September 5, 1992.

At the latitudinal band between 70°N and 75°N the gradient ratios are shown to be inversely proportional to the SAR backscatter. Between 75°N and 80°N the data points do not appear related and are basically random. Between 80°N and 85°N the gradient ratio varies quite a bit, while the SAR backscatter signatures were almost constant. The data points (between 80°N and 85°N) make it apparent why multiyear ice concentrations derived from the two sensors are different. In this case the mean SAR backscatter was close to −9.3 dB, while the gradient ratio varied between −0.063 and −0.098. A similar set of plots for the gradient ratios are shown in Figure 10. Here we plot the gradient ratio versus the SAR multiyear ice concentration instead of the SAR backscatter. The plot for all regions shows the nonlinearity in the relationship. At the latitudinal bands between 70°N and 75°N the gradient ratio does not appear to be sensitive to multiyear ice concentrations between 0 and 60%. Between 60 and 90% a strong linear relationship is apparent, but after 90% the gradient ratio is still strongly varying, while the SAR multiyear ice concentration was almost constant at about 95%.

Plots of 19-GHz and 37-GHz data versus the SAR backscatter are shown separately in Figures 9c and 9d, respectively.

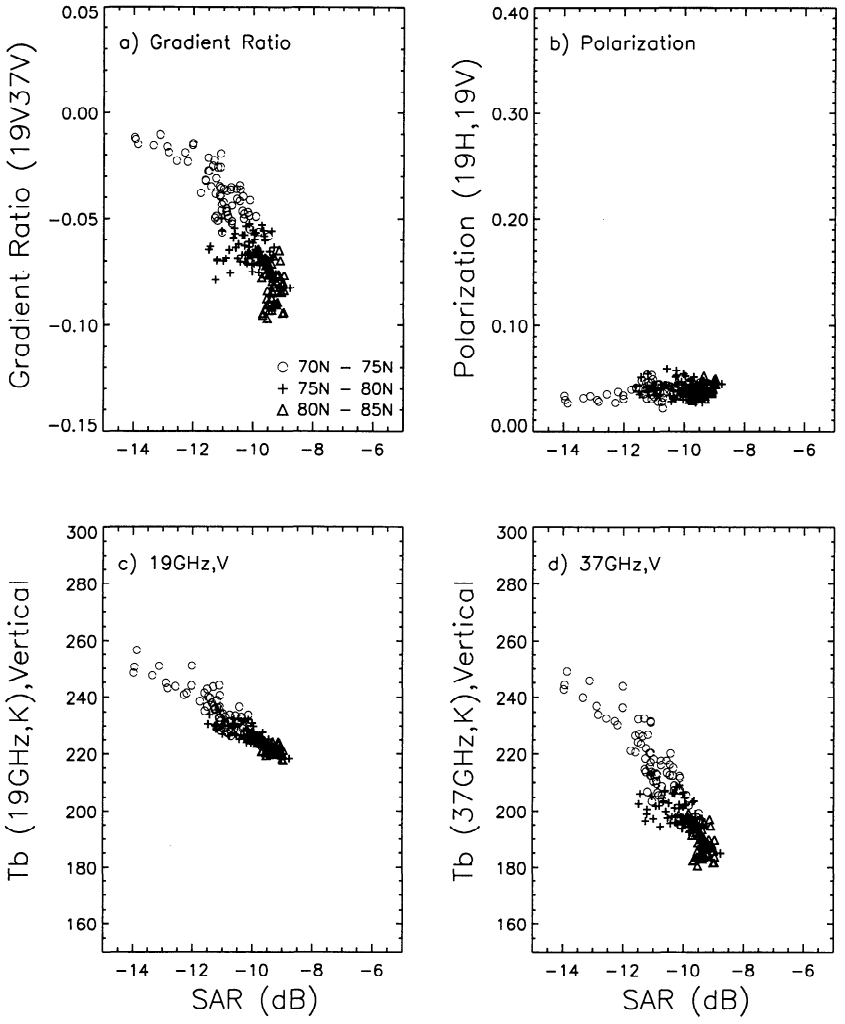

Figure 9. Comparison of SAR and passive microwave signatures at three latitudinal bands: (a) Gradient ratio versus SAR backscatter; (b) Polarization ratio versus SAR backscatter; (c) 19-GHz brightness temperature versus SAR backscatter; (d) 37-GHz brightness temperature versus SAR backscatter.

Data from the 19-GHz channel can be seen to be linearly related to the SAR backscatter at all latitudinal bands. At 80°N to 85°N the data indicate that both brightness temperature and backscatter are well defined. It is thus apparent that the use of 19 GHz alone to obtain multiyear ice concentration could provide results that are more consistent with the SAR data. The scatterplot of 37 GHz versus the SAR backscatter also shows approximately linear relationships, but it is clear that within the latitudinal range from 80°N to 85°N, the distribution of data is similar to the gradient ratio versus SAR distribution.

The good correlation of 19-GHz data with the SAR data brings in the question of whether snow cover is partly a reason for the lower values in the multiyear ice concentrations derived from passive microwave versus those from SAR. The SAR and the 19-GHz data are not as sensitive to snow as the 37-GHz data. While volume scattering in the multiyear ice may still be the dominant mode of scattering that enables discrimination of first-year ice from multiyear ice, the 37-GHz data may also reflect scattering of the 0.8-cm radiation with snow cover. Radiative transfer modeling studies of snow indicate that this effect is not negligible.

5. Summary/Discussion

Team Algorithm Estimates: Summary

Over the annual cycle the total ice concentration remained fairly high in our region of study. From the Team algorithm estimates we observe a significant decrease in the amount of multiyear ice (almost 40%) between January and April and a slower increase in the amount of multiyear ice between October and December. The multiyear ice concentration at freeze-up is much lower than the ice concentration at the end of summer, an inconsistency in the analysis which suggests an underestimation of multiyear ice in the winter time. Melt ponds and other surface effects seem to contribute significantly to the underestimation of ice concentration in the summer.

The Team algorithm seems to underestimate multiyear concentration. One possible reason is the low values of reference brightness temperatures of multiyear ice used by the algorithm. Because of the large variability of the emissivity of multiyear ice, the reference brightness temperature of multiyear ice appropriate for the entire Arctic region is difficult to establish. Another reason is having signatures similar to those of first-

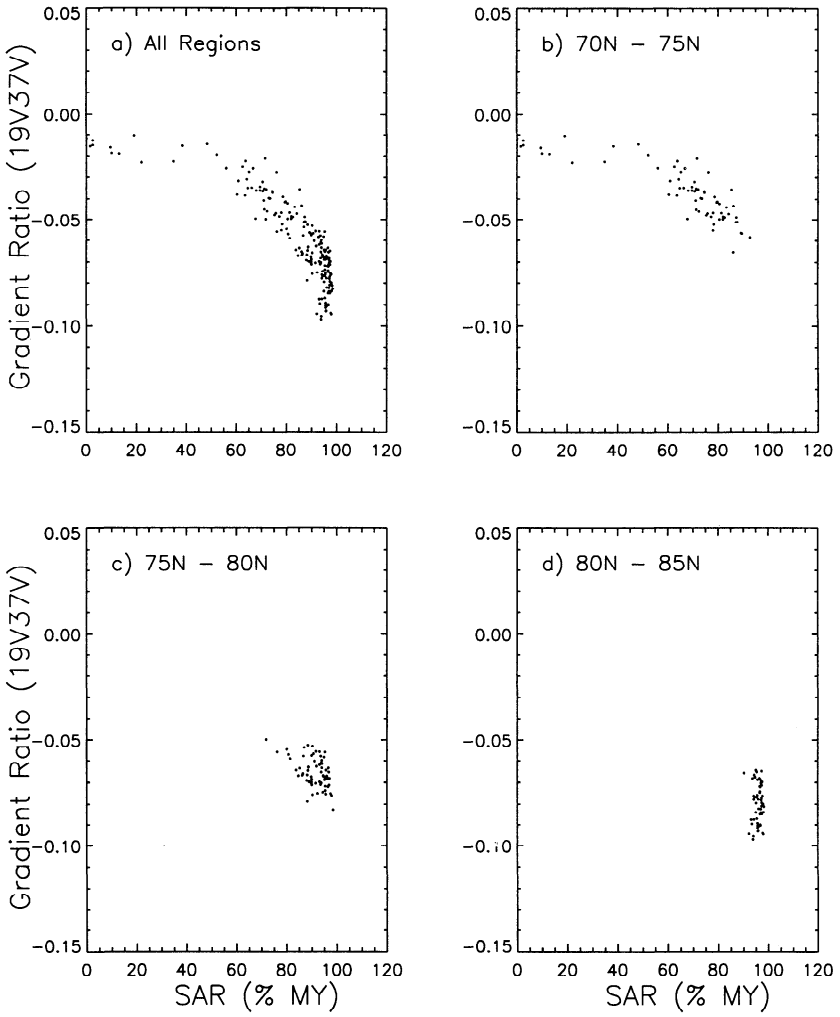

Figure 10. Scatterplot of gradient ratio at various latitude bands versus SAR multiyear ice concentration.

year ice. Observations have shown that frozen melt ponds can have signatures of first-year ice. Also, the snow/ice interfaces of previously flooded multiyear ice floes could have signatures of first-year ice because of relatively high salinity at the surface. Furthermore, second-year ice may have different emissivity than other types of multiyear ice, as has been previously observed [*Tooma et al.*, 1975]. Atmospheric water vapor, cloud liquid content, and wind [*Maslanik*, 1992] all contribute to the underestimation of multiyear ice by the Team algorithm.

SAR Estimates: Summary

The SAR analyses suggest a perennial ice cover in the Beaufort which is rather stable throughout a season. The amount of multiyear ice remained approximately constant, within the level of uncertainty of the analysis. The average multiyear ice concentration in this part of the Arctic Ocean is approximately 80%. The multiyear ice concentration is approximately equivalent to the ice concentration at the end of the summer. These analyses seem to give a consistent view of the annual cycle.

We have discussed the possible confusion for identification of multiyear ice and first-year ice in the winter Beaufort Sea. The results seem to indicate (discussed in the last section) that deformed first-year ice, within the level of uncertainty, does not contribute significantly to the overestimation of multiyear ice in SAR data even though their backscatter signatures might be similar. We note that ridged ice occupies a smaller area than the original undeformed ice such that contribution of ridged (deformed) first-year ice area to the total multiyear contribution may not be significant. However, we do not know the areal contribution of this misclassified ice type. The C band radar, to first order, is not affected by snow cover when the temperature is below freezing and is much less sensitive to weather effects than the higher-frequency radiometer channels. The equivalence between summer ice minima and winter multiyear ice concentration and the small fluctuations in the SAR estimates in the winter lead us to believe that these estimates are at least consistent.

Multiyear Ice Concentration

The significance of the multiyear ice in the Arctic Ocean can be attributed to its strong relation to the summer ice concentration [*Comiso*, 1990; *Rothrock and Thomas*, 1990]. If there are changes in the climate which cause persistent decrease in the summer ice concentration, it would be reflected in a decrease in the amount of multiyear ice in the winter. This reduction would be due to increased melt or export of ice from the Fram Strait. An accurate record of the multiyear ice balance and fluctuations would be important in understanding the relationship between climate and multiyear ice balance. It is also important to understand whether a thinning of the ice cover [*Wadhams*, 1990] occurs in a highly compact multiyear ice cover as revealed by SAR or in a much lower multiyear ice cover as inferred from SSMI data.

Rothrock and Thomas [1990] demonstrated that more multiyear ice is required to maintain consistency between the summer ice and winter multiyear ice concentrations. However, as they recognized, their Kalman filter smoother can insist on consistency but without providing more accurate estimates if the observations are biased. That is, the estimates themselves are biased. At this point the analysis of the SAR data offers another estimate of the multiyear ice, which seems to be consistent with the summer ice concentration. If the SAR is correct, then the Team algorithm underestimates the multiyear ice by even a larger amount than previous studies have shown and implies a higher multiyear ice concentration in the Beaufort Sea.

Melt Pond Fraction and Ice Extent

Because melt pools have signatures of open water and the Team algorithm does not discriminate between the two surface types, it underestimates the ice concentrations in the summer. If the melt pond concentration is 30%, then the ice concentration would be underestimated by a similar amount. This is consistent with the differences between the SAR analysis and the Team algorithm analysis: the SAR estimates of total ice concentration are always higher than those of the Team algorithm in the summer. These differences are also larger at the lower-latitude bands, suggesting that melt pond fraction is dependent on latitude and proximity to the coast (I. P. Romanov, unpublished manuscript, 1993). If the Team algorithm underestimates the total ice concentration due to melt ponds, especially in the ice margin in the summer, then the computed total ice area would also be underestimated.

Summary Remarks

The estimates from the SAR and Team algorithms provided two fairly different views of the Beaufort Sea ice cover. The limitations of both algorithms were discussed. The differences explain some of the possible biases of these algorithms due to variability in signature as functions of wavelength and environmental conditions. Future investigations using these data sets should be cautious of the possible biases introduced by these analysis algorithms.

Acknowledgments. We would like to thank Rico Allegrino of Hughes STX for his assistance in programming and analysis of the data. R. Kwok and G. F. Cunningham performed this work at the Jet Propulsion Laboratory, California Institute of Technology, under contract with the National Aeronautics and Space Administration. J. C. Comiso performed this work at the Laboratory for Hydrospheric Processes at NASA Goddard Space Flight Center. This project was supported by the NASA Cryospheric Processes Program under R. H. Thomas.

References

Carsey, F. D., Arctic sea ice distribution at end of summer from satellite microwave data, *J. Geophys. Res.*, *87*(C8), 5809–5835, 1982.

Cavalieri, D. J., The validation of geophysical products using multisensor data, in *Microwave Remote Sensing of Sea Ice*, *Geophys. Monogr. Ser.*, vol. 68, edited by F. D. Carsey, pp. 233–242, AGU, Washington, D. C., 1992.

Cavalieri, D. J., P. Gloersen, and W. J. Campbell, Determination of sea ice parameters from Nimbus 7 SMMR, *J. Geophys. Res.*, *89*(D4), 5355–5369, 1984.

Cavalieri, D. J., J. P. Crawford, M. R. Drinkwater, D. T. Eppler, L. D. Farmer, R. R. Jentz, and C. C. Wackerman, Aircraft active and passive validation of sea ice concentration from the Defense Meteorological Satellite Program Special Sensor Microwave Imager, *J. Geophys. Res.*, *96*(C12), 21,989–22,008, 1991.

Comiso, J. C., Sea ice microwave emissivities from satellite passive microwave and infrared observations, *J. Geophys. Res.*, *88*(C12), 7686–7704, 1983.

Comiso, J. C., Arctic multiyear ice classification and summer ice cover using passive microwave satellite data, *J. Geophys. Res.*, *95*(C8), 13,411–13,422, 1990.

Comiso, J. C., SSM/I Ice concentrations using the bootstrap algorithm, *NASA Publ.*, *RP-1380*, 50 pp., 1995.

Comiso, J. C., and R. Kwok, Surface and radiative characteristics of the summer Arctic sea ice cover from multisensor satellite observations, *J. Geophys. Res.*, this issue.

Fetterer, F., D. Gineris, and R. Kwok, Sea ice type maps from Alaska synthetic aperture radar facility imagery: An assessment, *J. Geophys. Res.*, *99*(C11), 22,443–22,458, 1994.

Gloersen, P., and D. J. Cavalieri, Reduction of weather effects in the calculation of sea ice concentration from microwave radiances, *J. Geophys. Res.*, *91*(C3), 3913–3919, 1986.

Grenfell, T. C., Surface-based passive microwave studies of multiyear ice, *J. Geophys. Res.*, *97*(C3), 3485–3501, 1992.

Grenfell, T. C., and A. W. Lohanick, Temporal variations of the microwave signatures of sea ice during the late spring and early summer near Mould Bay NWT, *J. Geophys. Res.*, *90*(C3), 5063–5074, 1985.

Kwok, R., and G. F. Cunningham, Backscatter characteristics of the winter sea ice cover in the Beaufort Sea, *J. Geophys. Res.*, *99*(C4), 7787–7803, 1994a.

Kwok, R., and G. F. Cunningham, Use of time series SAR data to resolve ice type ambiguities in newly-opened leads, in *Proceedings of IGARSS'94*, pp. 1024–1026, Inst. of Electrical and Electronics Eng., Piscataway, N. J., 1994b.

Kwok, R., E. Rignot, B. Holt, and R. G. Onstott, Identification of sea ice types in space-borne SAR data, *J. Geophys. Res.*, *97*(C2), 2391–2402, 1992.

Maslanik, J. A., Effects of weather on the retrieval of sea ice concentration and ice type from passive microwave data, *Int. J. Remote Sens.*, *13*(1), 37–54, 1992.

Nakamura, N., and A. H. Oort, Atmospheric heat budget of the polar regions, *J. Geophys. Res.*, *93*(D8), 9510–9524, 1988.

Rignot, E., and M. Drinkwater, Winter sea ice mapping from multiparameter synthetic aperture radar, *J. Glaciol.*, *40*, 31–45, 1994.

Rothrock, D. A., and D. R. Thomas, The Arctic Ocean multiyear ice balance, 1979–82, *Ann. Glaciol.*, *14*, 252–255, 1990.

Steffen, K., and J. Heinrichs, Feasibility of sea ice typing with synthetic aperture radar (SAR): Merging of Landsat thematic mapper and ERS 1 satellite imagery, *J. Geophys. Res.*, *99*(C11), 22,413–22,424, 1994.

Steffen, K., J. Key, D. J. Cavalieri, J. Comiso, P. Gloersen, K. St. Germain, and I. Rubenstein, The estimation of geophysical parameters using passive microwave algorithms, in *Microwave Remote Sensing of Sea Ice*, *Geophys. Monogr. Ser.*, vol. 68, edited by F. D. Carsey, pp. 201–232, AGU, Washington, D. C., 1992.

Thomas, D. R., Arctic sea ice signatures for passive microwave algorithms, *J. Geophys. Res.*, *98*(C6), 10,037–10,052, 1993.

Thomas, D. R., and D. A. Rothrock, The Arctic Ocean ice balance: A Kalman filter smoother estimate, *J. Geophys. Res.*, *98*(C6), 10,054–10,067, 1993.

Thorndike, A. S., D. A. Rothrock, G. A. Maykut, and R. Colony, The thickness distribution of sea ice, *J. Geophys. Res.*, *80*(33), 4501–4512, 1975.

Tooma, S. G., R. A. Mannella, J. P. Hollinger, and R. D. Ketchum Jr., Comparison of sea ice type identification between airborne dual frequency passive microwave radiometry and standard laser/infrared techniques, *J. Glaciol.*, *15*, 225–239, 1975.

Wadhams, P., Evidence for thinning of ice cover north of Greenland, *Nature*, *345*, 795–797, 1990.

Wittmann, W. I., and J. Schule Jr., Comments on the mass budget of Arctic ice pack, in *Proceedings of the Symposium on the Arctic Heat Budget and Atmospheric Circulation*, edited by J. O. Fletcher, *Memo. RM-5233-NSF*, pp. 215–246, Rand Corp., Santa Monica, Calif., 1966.

J. C. Comiso, Laboratory for Hydrospheric Processes, NASA Goddard Space Flight Center, Greenbelt, MD 20771.

G. F. Cunningham and R. Kwok, Jet Propulsion Laboratory, California Institute of Technology, 4800 Oak Grove Drive, Pasadena, CA 91109. (e-mail: ron@rgps1.jpl.nasa.gov)

(Received February 5, 1996; revised June 17, 1996;
accepted June 22, 1996.)